Introduction to Nanotechnology and Nanoscience – Class#5

Liwei Lin

Professor, Dept. of Mechanical Engineering
Co-Director, Berkeley Sensor and Actuator Center
The University of California, Berkeley, CA94720
e-mail: lwlin@me.berkeley.edu
http://www.me.berkeley.edu/~lwlin

Outline

- Top-down Technologies
- MOSFET (review)
- FINFET
- Paper #1 and Paper #1-1

- (some materials from Professors Lydia Sohn & Tsu-Jae King Liu)

Intel: Lunar Lakes Tapes Out, Meteor Lake on Track for 2023 Ramp

By Anton Shilov published 4 days ago **2022**

Meteor Lake to ramp in 2023, Lunar Lake ready for production in 2024.

Meteor Lake is an important milestone for Intel for two reasons: it is the company's first client CPU to rely on a disaggregated multi-tile design, and it is the first to use the Intel 4 process technology (aka 7nm), which is Intel's first node to use extreme ultraviolet (EUV) lithography. The system-in-package will consist of four tiles: the compute tile (CPU cores), the graphics tile produced by TSMC (presumably using its N3 or N5 node)

Scalable Architecture across Multiple Generations

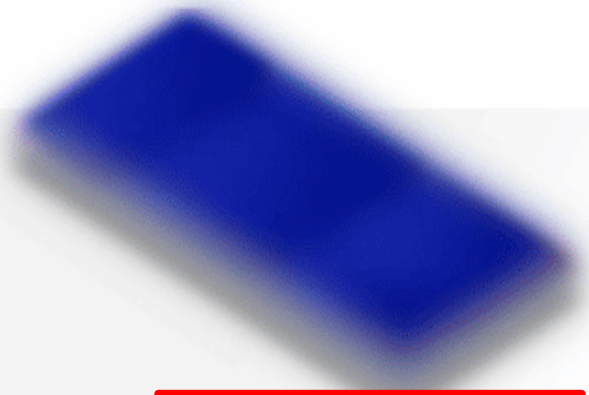

	Meteor Lake	Arrow Lake	Lunar Lake & Beyond
Packaging	▪ Foveros ▪ 36 µm pitch	▪ Foveros ▪ 36 µm pitch	▪ Foveros ▪ 25 µm pitch
Process	Intel 4 / External	Intel 20A / External	Intel Next / External

HOT CHIPS

intel. 36

Carrier Drift across the Junction

- Because charge density ≠ 0 in the depletion region, an electric field exists, hence there is drift current.

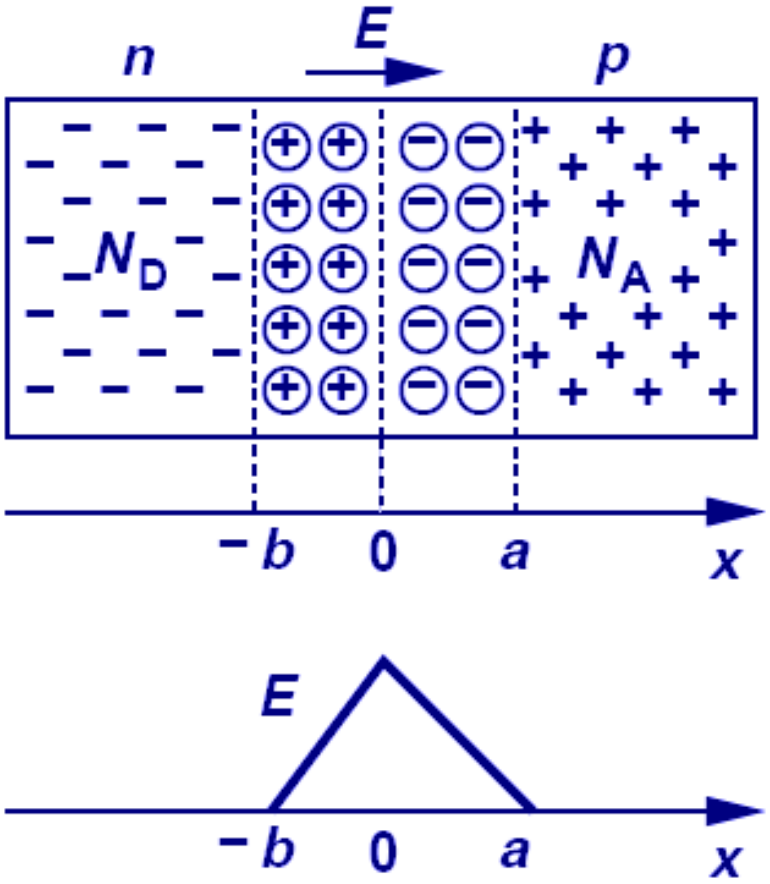

Reverse Breakdown

- As the reverse bias voltage increases, the electric field in the depletion region increases. Eventually, it can become large enough to cause the junction to break down so that a large reverse current flows:

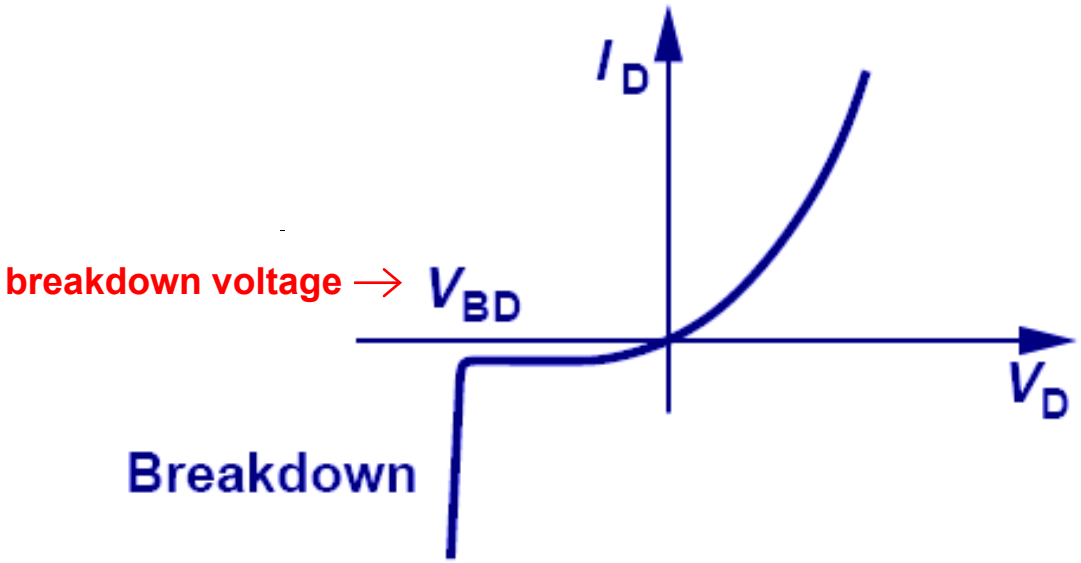

The MOSFET

Metal-Oxide-Semiconductor Field-Effect Transistor:

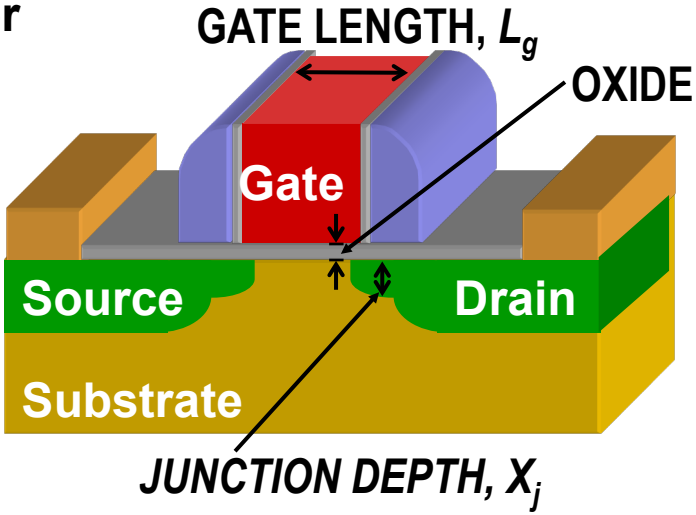

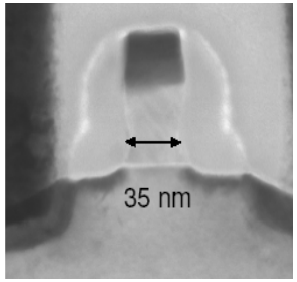

M. Bohr, *Intel Developer Forum*, September 2004

- Current flowing through the **channel** between the **source** and **drain** is controlled by the **gate** voltage.

- **"N-channel" & "P-channel" MOSFETs operate in a complementary manner**
  "CMOS" = Complementary MOS

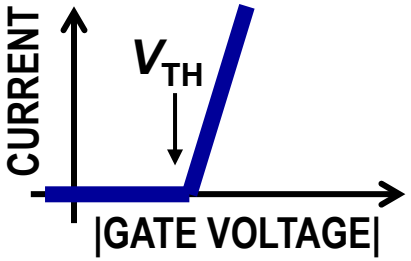

N-Channel MOSFET Structure

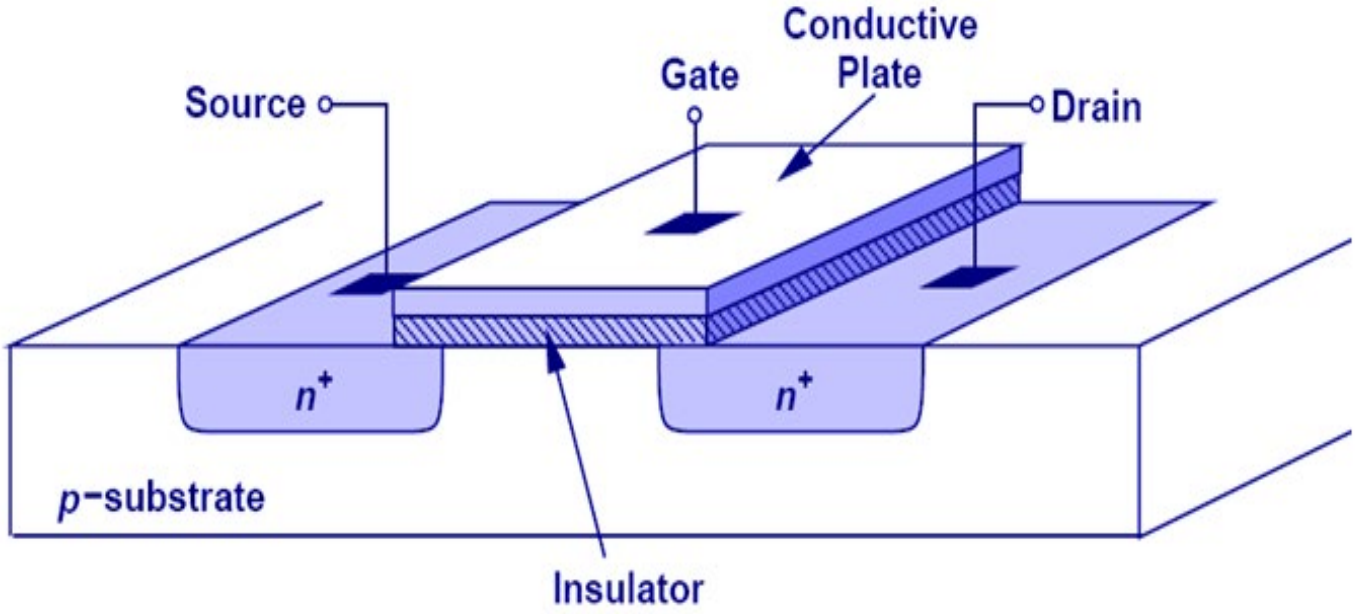

Circuit symbol

- The conventional gate material is heavily doped polycrystalline silicon (referred to as "polysilicon" or "poly-Si" or "poly")
  - Note that the gate is usually doped the same type as the source/drain, *i.e.* the gate and the substrate are of opposite types.
- The conventional gate insulator material is SiO_2.
- To minimize current flow between the substrate (or "body") and the source/drain regions, the p-type substrate is grounded.

Channel Formation (Qualitative)

- As the gate voltage (V_G) is increased, holes are repelled away from the substrate surface.
  - The surface is depleted of mobile carriers. The charge density within the ***depletion region*** is determined by the dopant ion density.

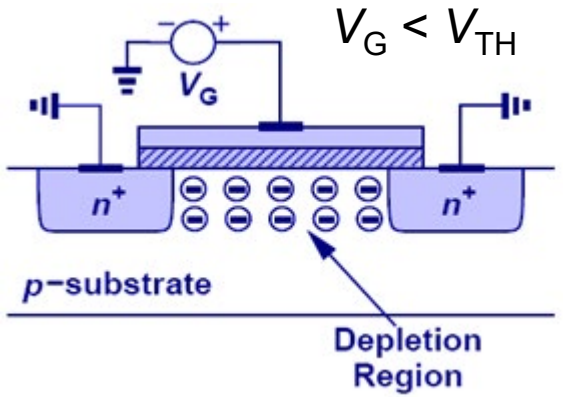

- As V_G increases above the **threshold voltage V_{TH},** a layer of conduction electrons forms at the substrate surface.
  - For $V_G > V_{TH}$, $n > N_A$ at the surface.

  → **The surface region is "inverted" to be n-type.**

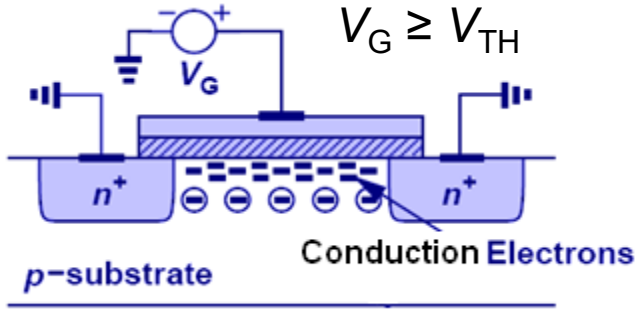

The electron ***inversion layer*** serves as a resistive path (***channel***) for current to flow between the heavily doped (*i.e.* highly conductive) ***source*** and ***drain*** regions.

Voltage-Dependent Resistor

- In the ON state, the MOSFET channel can be viewed as a resistor.

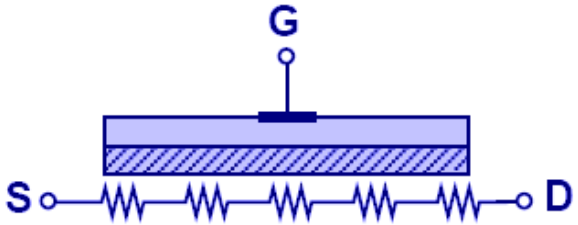

- Since the mobile charge density within the channel depends on the gate voltage, the channel resistance is voltage-dependent.

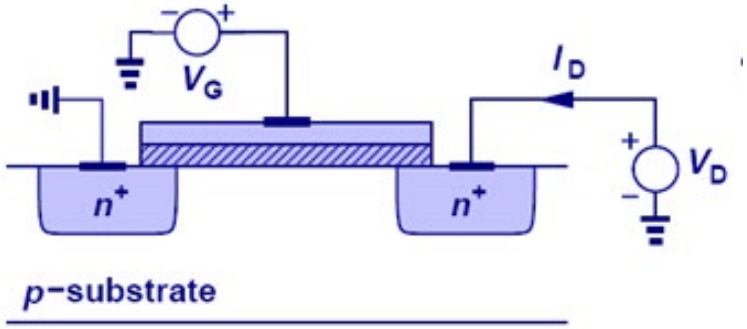

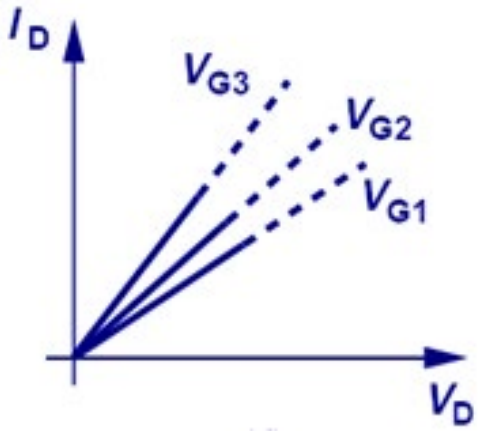

Channel Length & Width Dependence

- Shorter channel length and wider channel width each yield lower channel resistance, hence larger drain current.
  - Increasing *W* also increases the gate capacitance, however, which limits circuit operating speed (frequency).

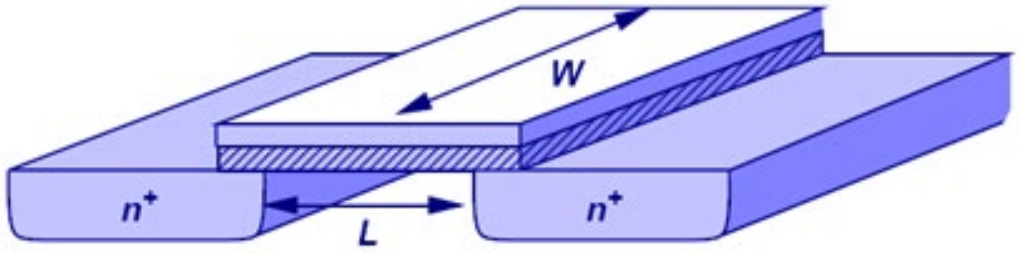

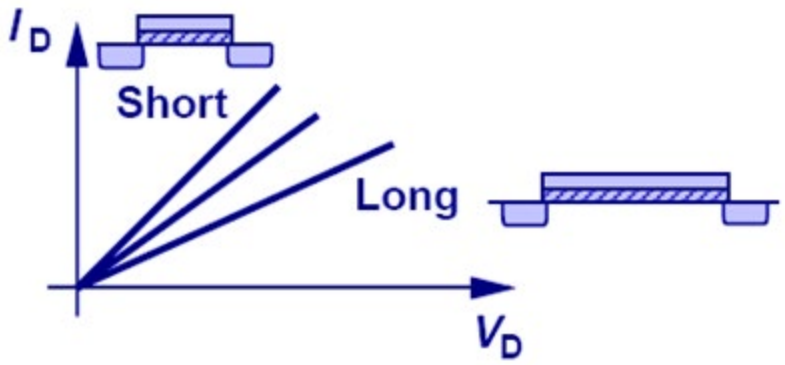

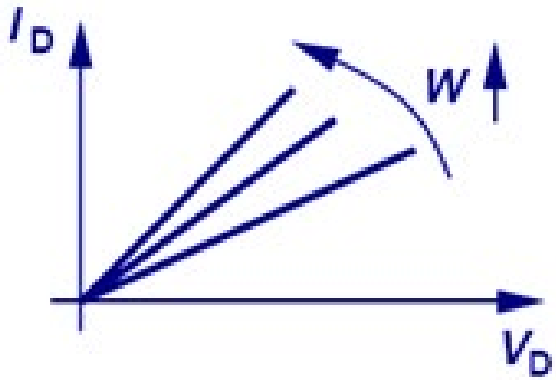

Charge in an N-Channel MOSFET

$V_{GS} < V_T$:

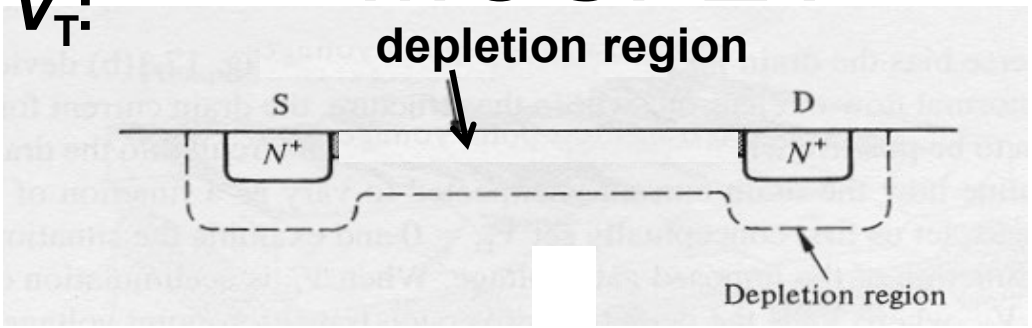

(no inversion layer at surface)

$V_{GS} > V_T$:

$V_{DS} \approx 0$

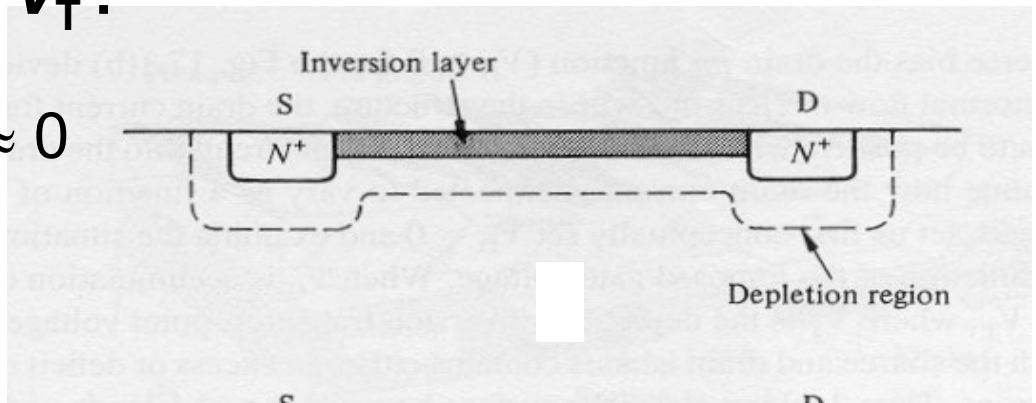

$V_{DS} > 0$ (small)

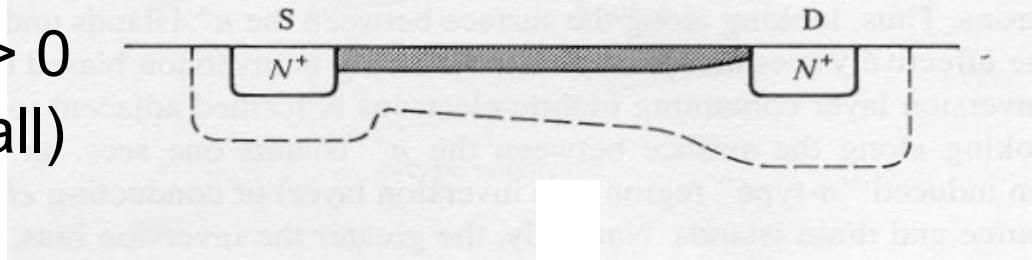

What Happens at Larger V_{DS}?

$V_{GS} > V_T$:

$V_{DS} = V_{GS} - V_T$

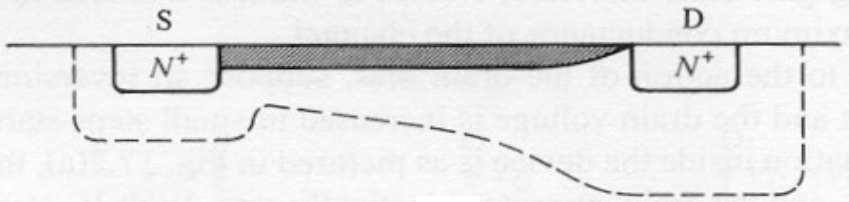

Inversion-layer is "pinched-off" at the drain end

$V_{DS} > V_{GS} - V_T$

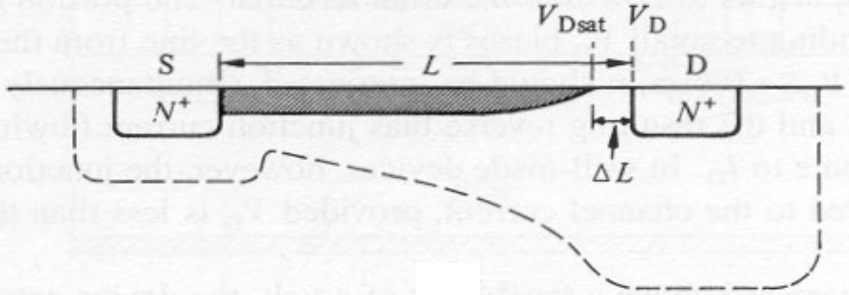

As V_{DS} increases above $V_{GS} - V_T \equiv V_{DSAT}$, the length of the "pinch-off" region ΔL increases:

- **"extra" voltage ($V_{DS} - V_{Dsat}$) is dropped across the distance ΔL**
- **the voltage dropped across the inversion-layer "resistor" remains V_{Dsat}**

  $\Rightarrow$ the drain current I_D saturates

Note: Electrons are swept into the drain by the *E*-field when they enter the pinch-off region.

Summary of I_D vs. V_{DS}

- As V_{DS} increases, the inversion-layer charge density at the drain end of the channel is reduced; therefore, I_D does not increase linearly with V_{DS}.
- When V_{DS} reaches $V_{GS} - V_T$, the channel is "pinched off" at the drain end, and I_D saturates (*i.e.* it does not increase with further increases in V_{DS}).

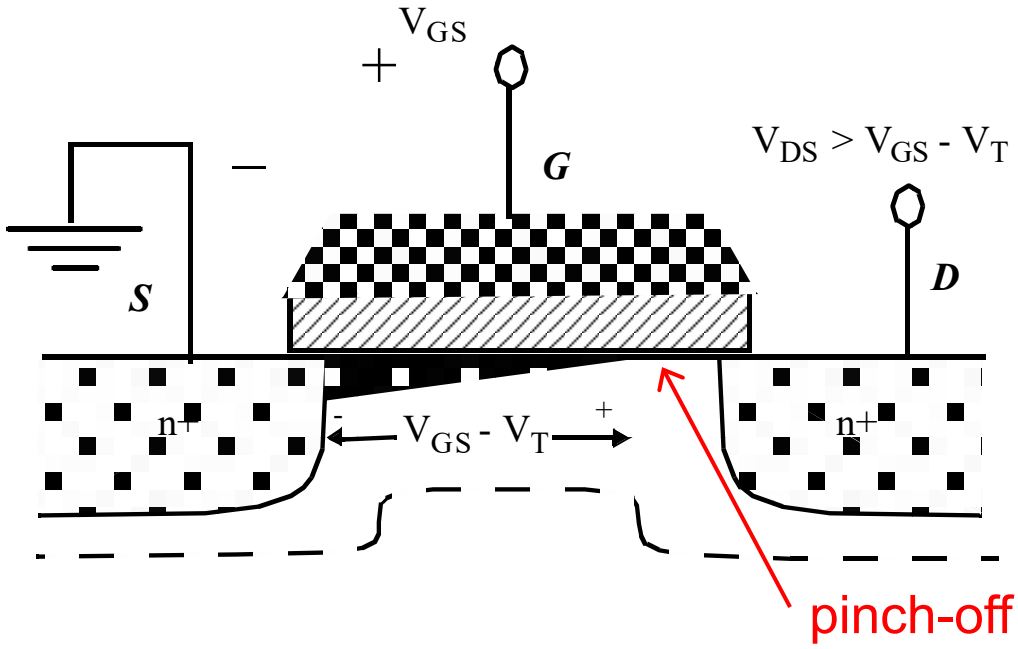

$$I_{DSAT} = \mu_n C_{ox} \frac{W}{2L}\left(V_{GS} - V_T\right)^2$$

Water Analogy of MOSFET

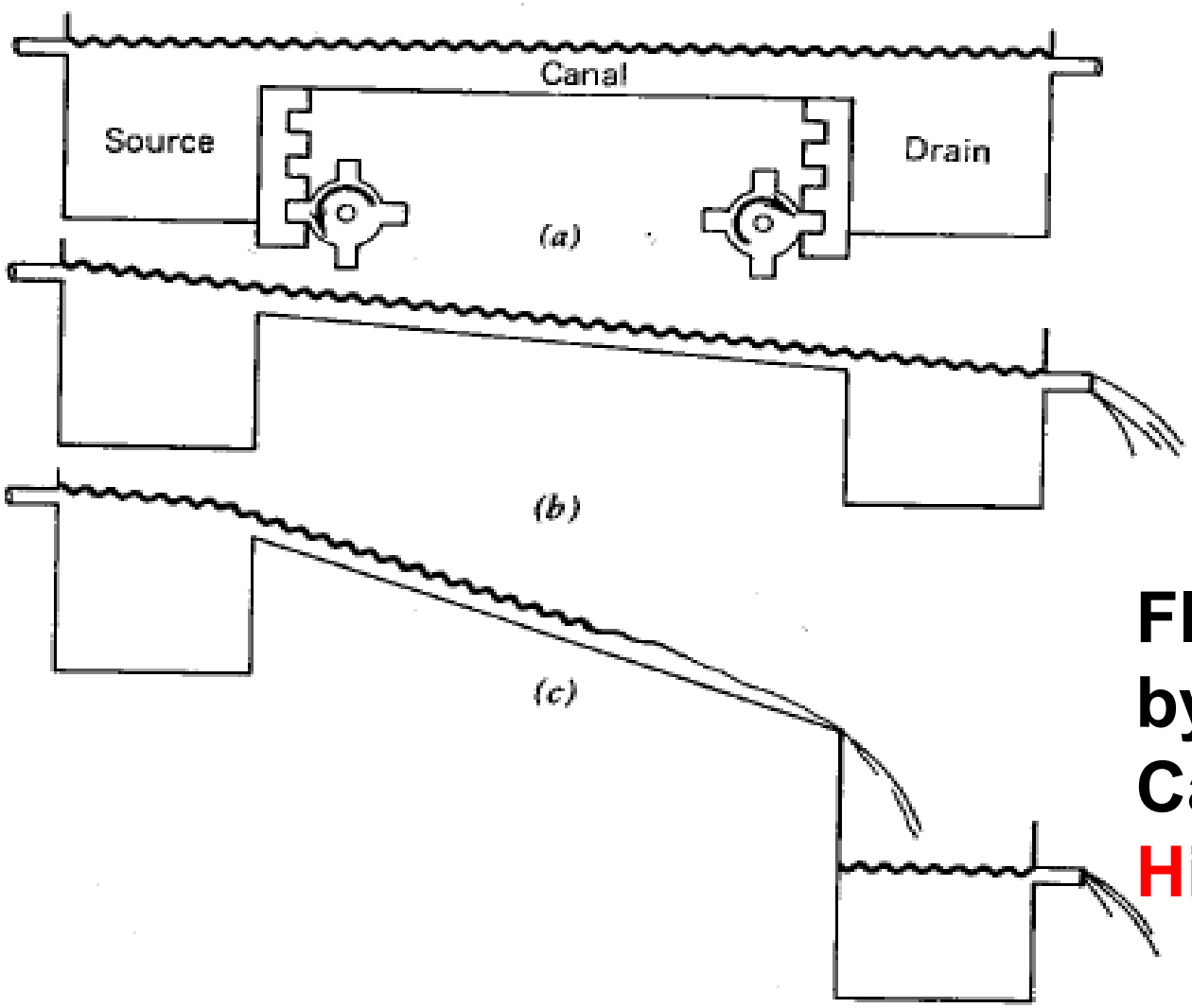

$V_D = V_S$

No water flow (current)

Lower Drain water flow

Flow is limited by the channel Capacity → Highest current

Drain Current Saturation

(Long-Channel MOSFET)

□ For $V_{DS} > V_{GS}-V_{TH}$: $I_D = I_{D,sat} = \frac{1}{2}\mu_n C_{ox}\frac{W}{L}(V_{GS}-V_{TH})^2$

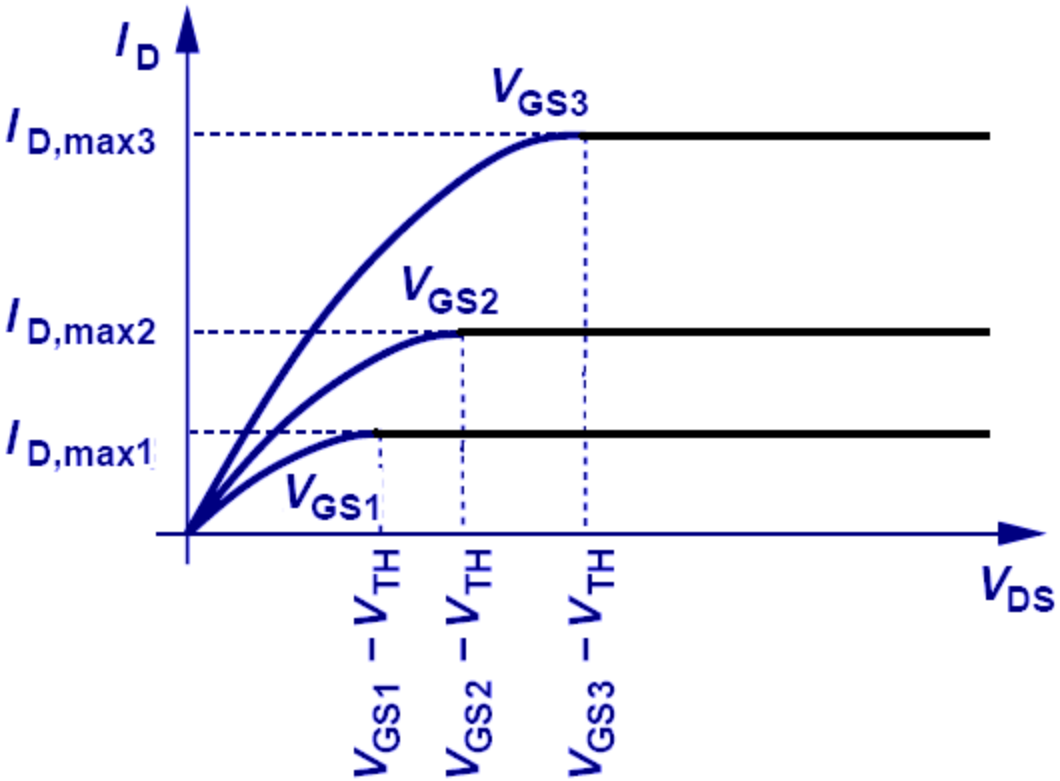

$$V_{D,sat} = V_{GS} - V_{TH}$$

MOSFET Regions of Operation (NMOS)

- When the potential difference between the gate and drain is greater than V_{TH}, the MOSFET is operating in the ***triode region***.
- When the potential difference between the gate and drain is equal to or less than V_{TH}, the MOSFET is operating in the ***saturation region***.

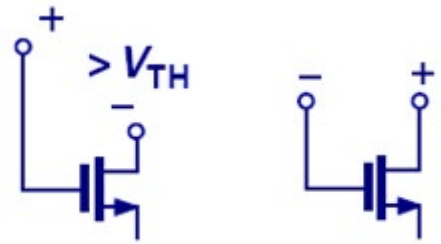

Gate capacitance

$$\frac{1}{2}\mu_n C_{ox}\frac{W}{L}(V_{GS}-V_{TH})^2$$

Electron mobility

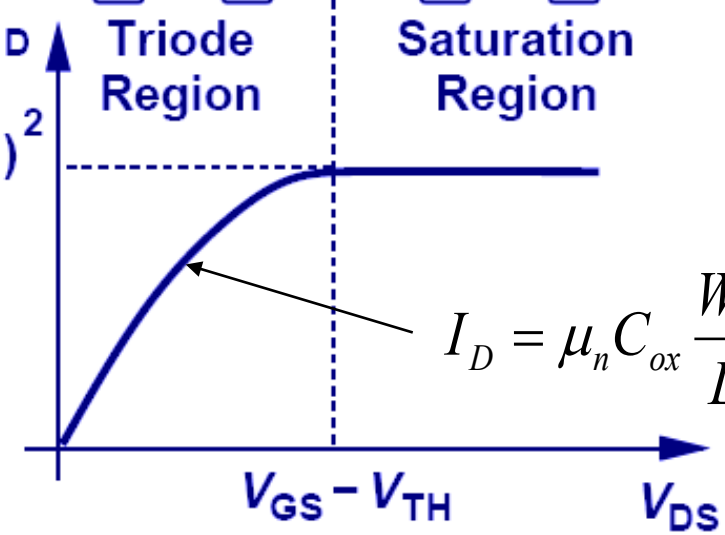

$$I_D = \mu_n C_{ox}\frac{W}{L}\left[(V_{GS}-V_{TH})-\frac{V_{DS}}{2}\right]V_{DS}$$

PMOS Transistor

- A p-channel MOSFET behaves similarly to an n-channel MOSFET, except the polarities for I_D and V_{GS} are reversed.

Schematic cross-section

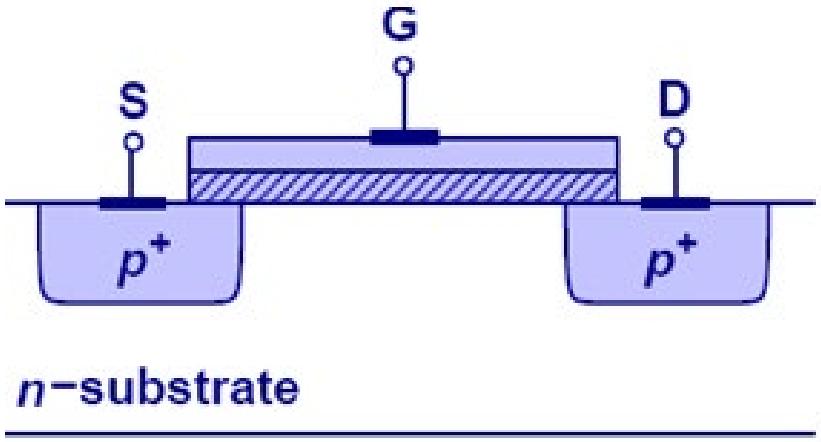

Circuit symbol

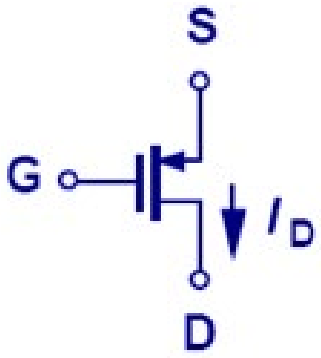

- The small-signal model for a PMOSFET is the same as that for an NMOSFET.
  - The values of g_m and r_o will be different for a PMOSFET *vs.* an NMOSFET, since mobility & saturation velocity are different for holes *vs*. electrons.

CMOS Technology

- It possible to form deep n-type regions ("well") within a p-type substrate to allow PMOSFETs and NMOSFETs to be co-fabricated on a single substrate.
- This is referred to as CMOS ("Complementary MOS") technology.

Schematic cross-section of CMOS devices

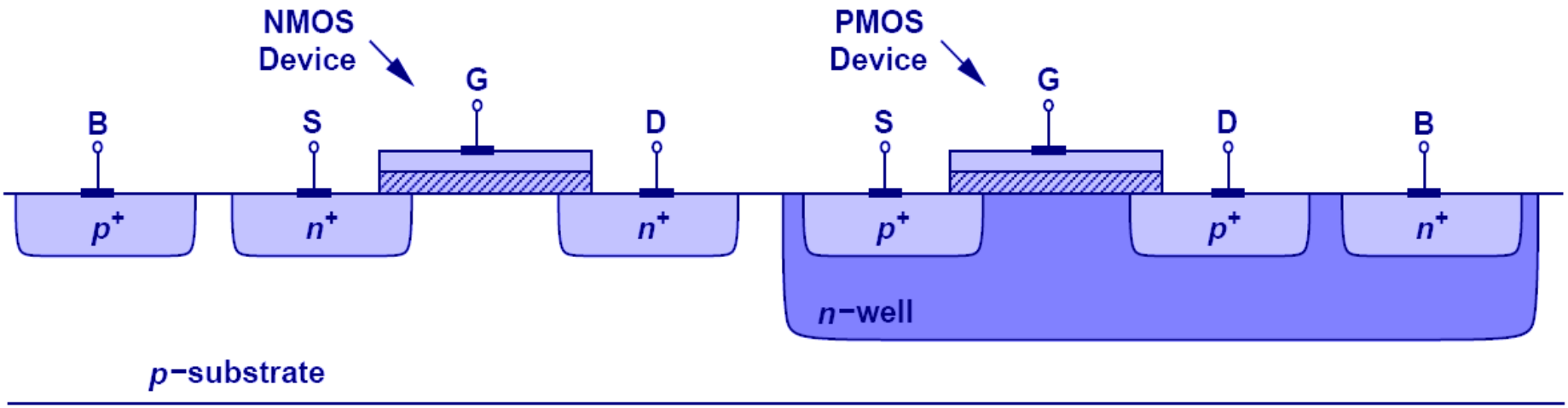

FinFET- Why and How (from Prof. C. Hu)

May 4, 2011, New York Times front page

- **Intel will use 3D FinFET at 22nm**
- **Most radical changes in decades**
- **There is a competing SOI technology**

Oxidation in NMOS

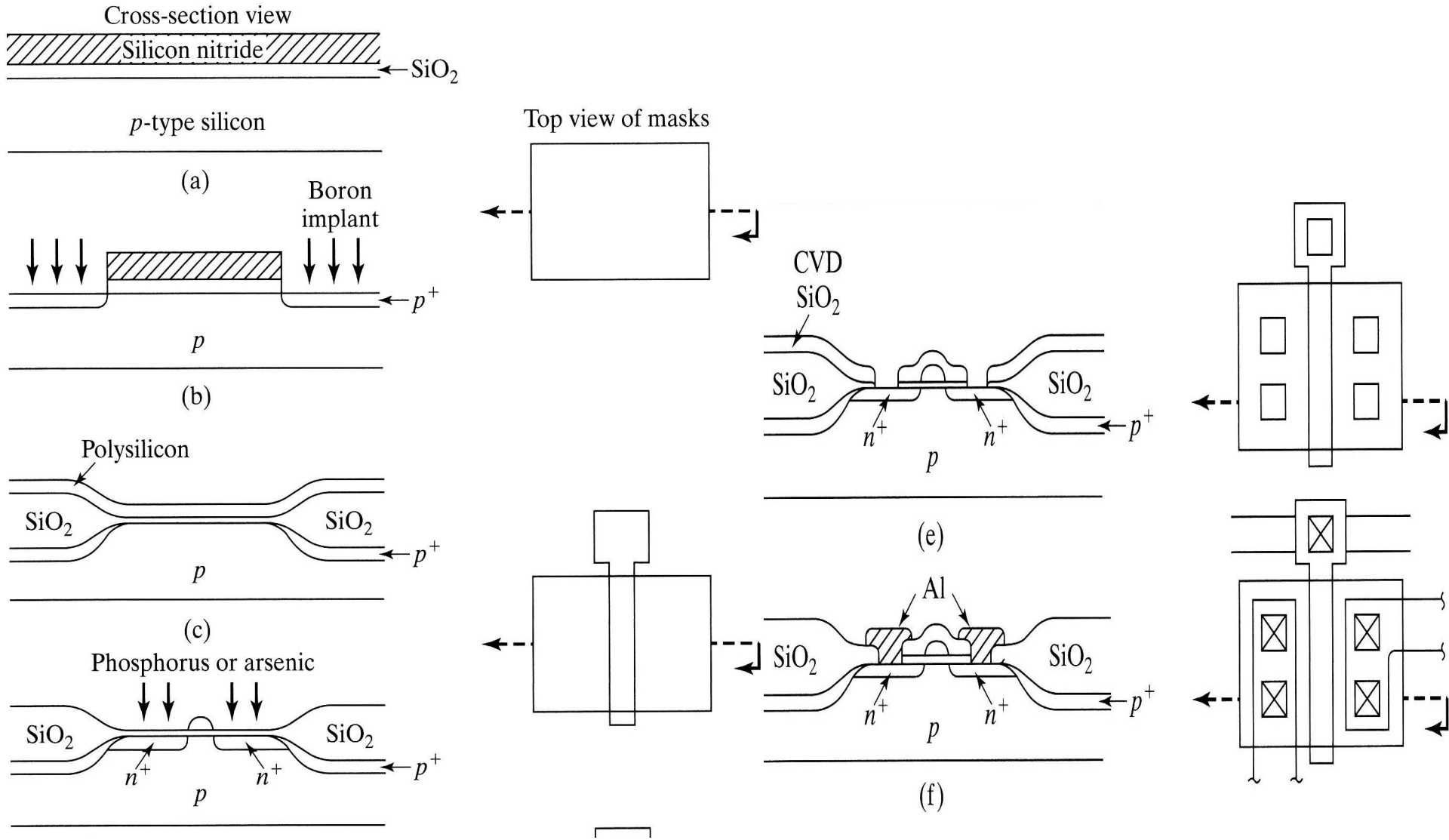

Good Old MOSFET Nearing Limits

- Reducing T_{ox} gives the gate excellent control of Si surface potential.
- But, the drain could still have more control than the gate along sub-surface leakage current paths. (Right figure.)

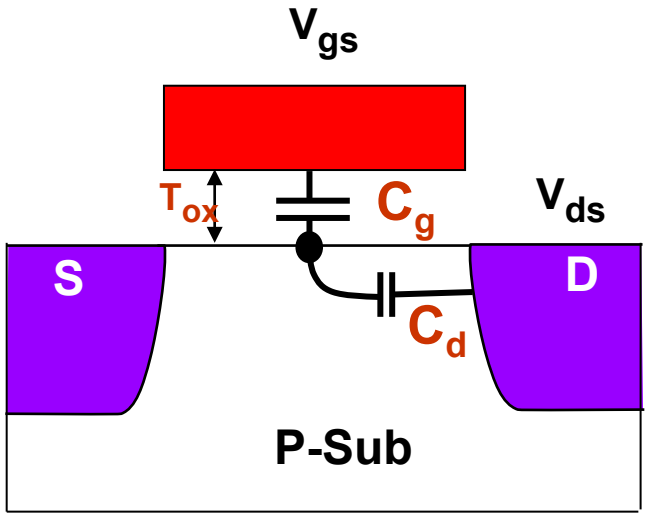

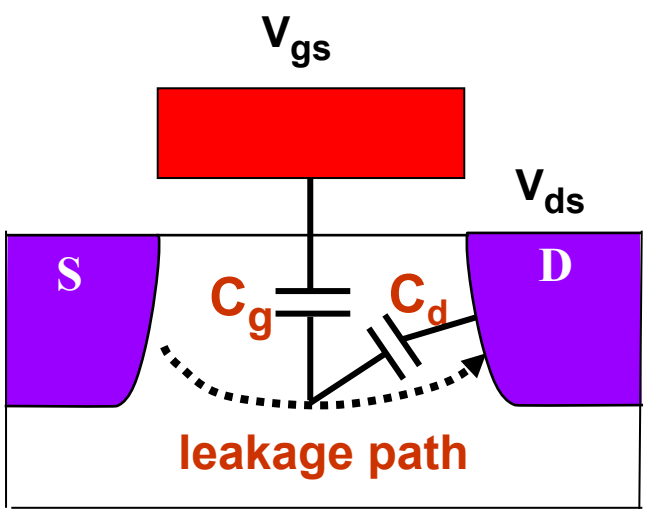

Ioff Got Worse at Smaller Length?

- **MOSFET becomes "resistor" at very small L**
- **Gate can't control the leakage current that are far away from the gate**

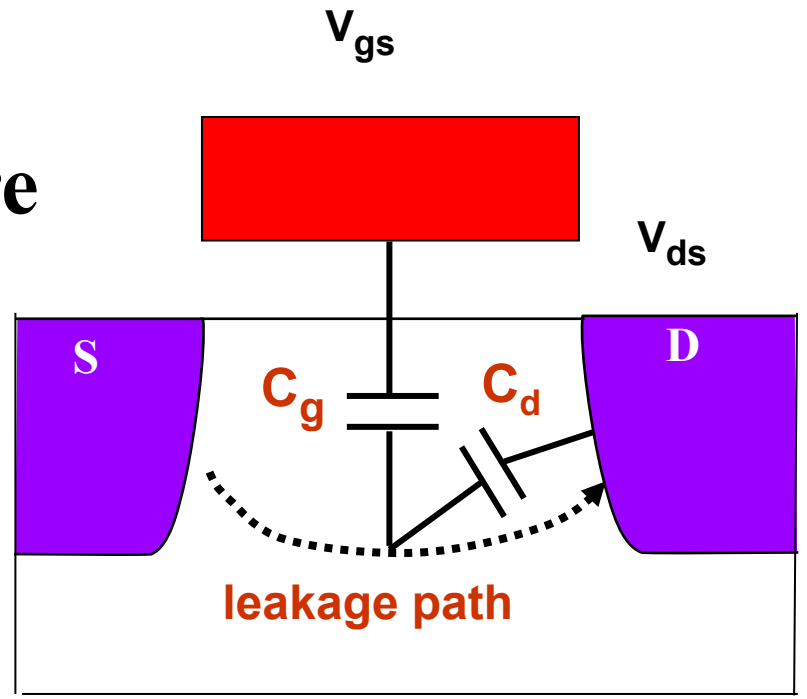

Introduction

First FinFET - DELTA (DEpleted Lean-channel TrAnsistor)

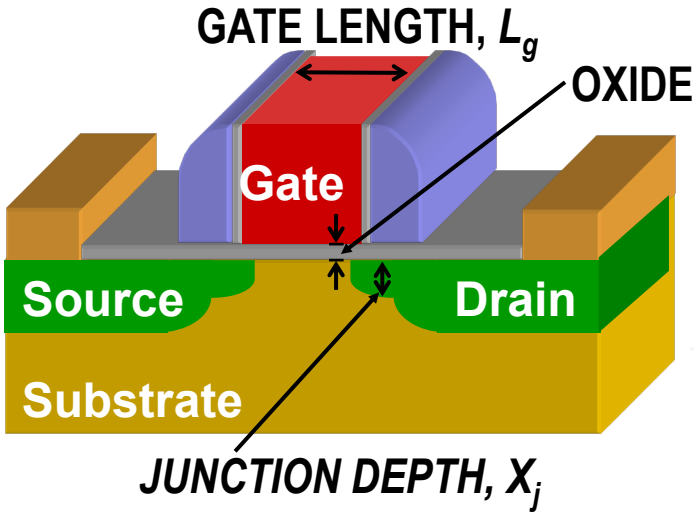

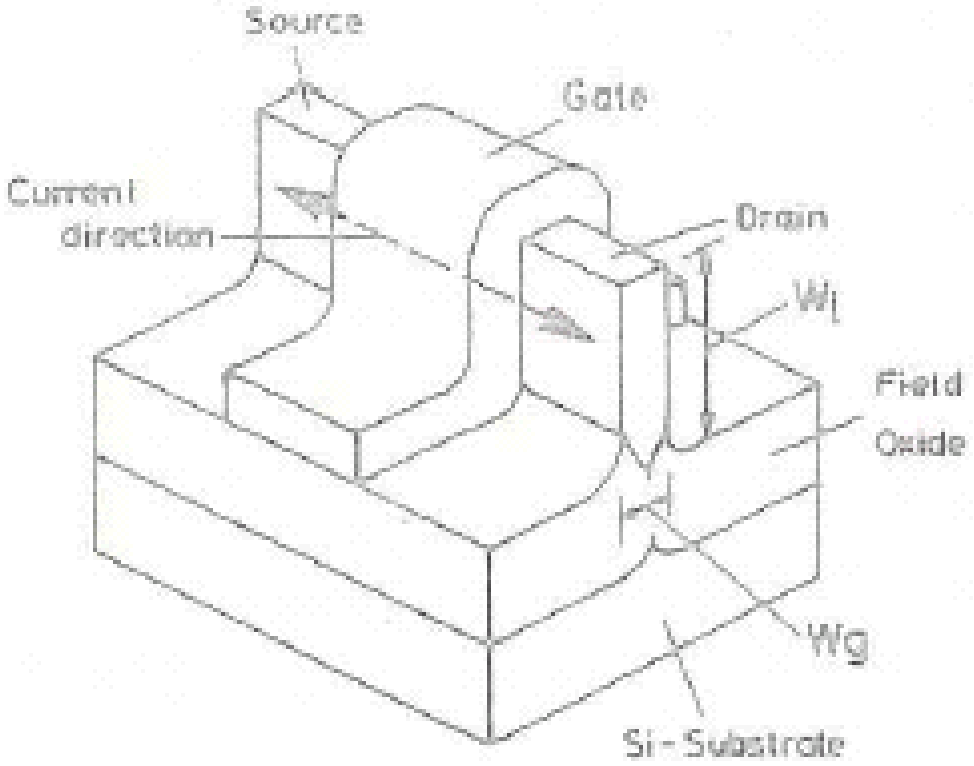

D.Hisamoto, T.Kaga, Y.Kawamoto, and E.Takeda, *IEEE Electron Dev. Lett.*, vol.11, no.1, p36-38, Jan 1990

New MOSFET Structure

FinFET

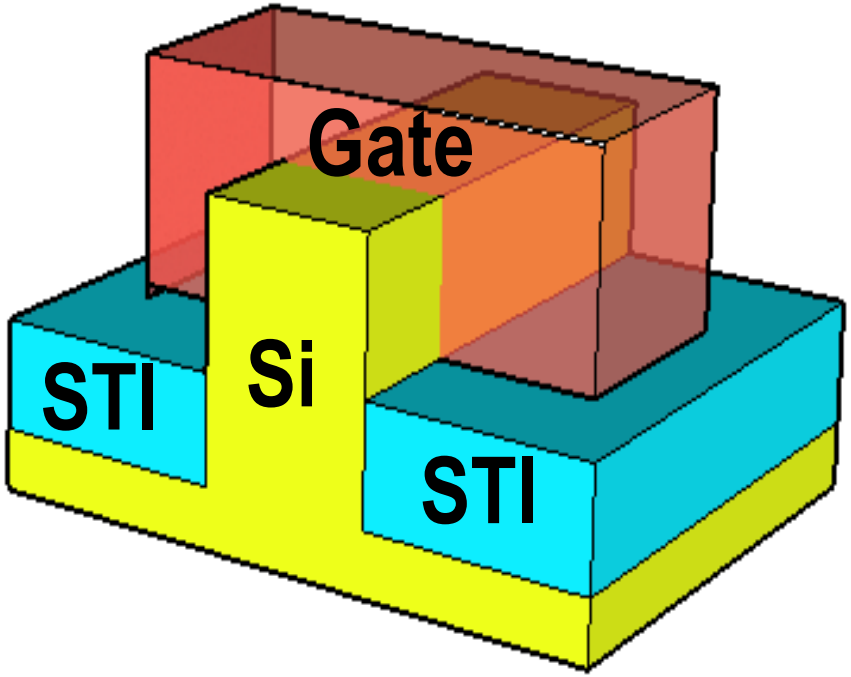

Ultra-Thin Body SOI

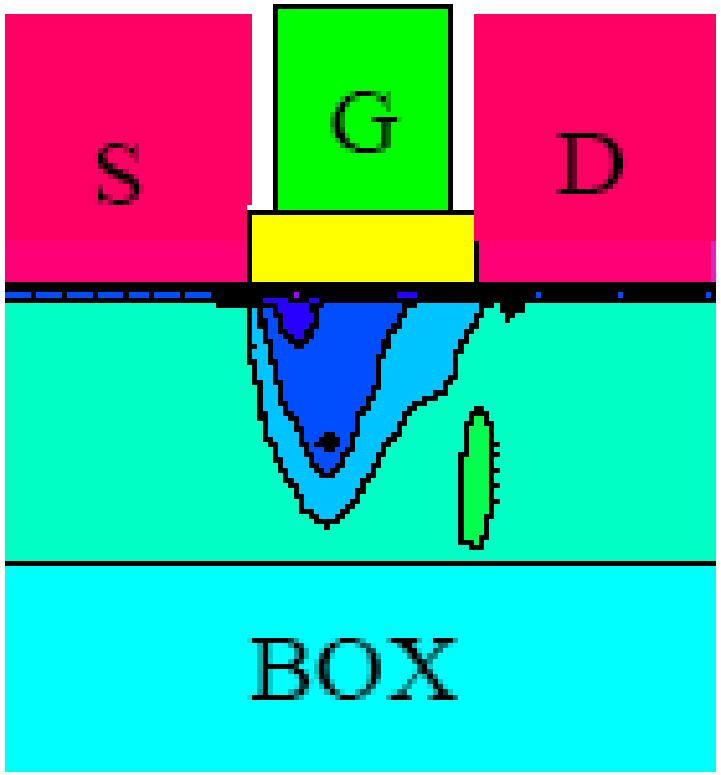

shallow trench isolation (**STI**)

GAAFET Structure

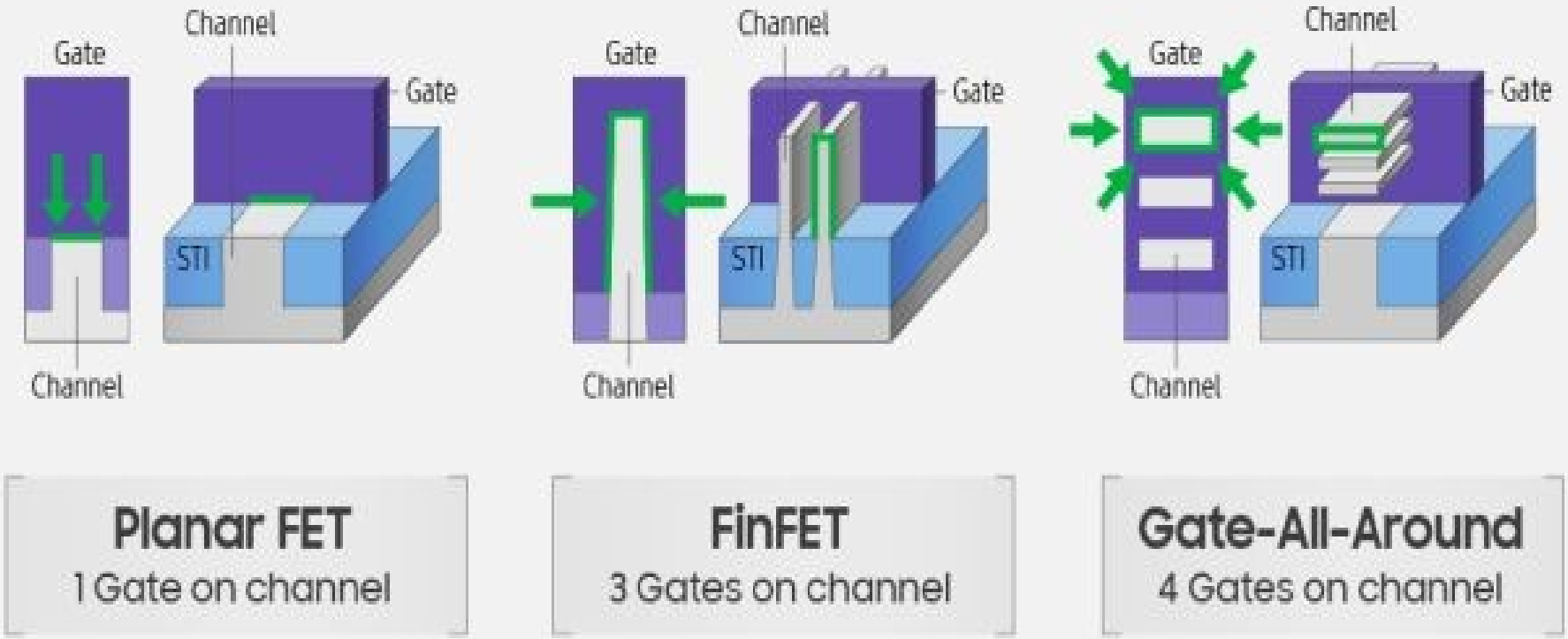

HARDWARE

Samsung Makes the First 3nm GAAFET Semiconductor!

By Evan Federowicz

Jan 4, 2020 22:33 EST

The 3 nm process is based around the Gate All Around (GAAFET) technology, which is different from the industry standard of FinFET. This change in technology reduces the total silicon size by 35% while taking less 50% less power as well. This allows for a 33% performance increase over the 5 nm FinFET process.

When Samsung originally started working on the 3 nm GAAFET process a year ago, this 3 nm GAAFET process had initially been planned to begin mass production in 2021. This comes in the wake of the 7 nm commercial peak with AMD using this process in the creation of the Ryzen 3000 series.

Beyond 3 nm

The ITRS uses (as of 2017) the terms "2.1 nm", "1.5 nm", and "1.0 nm" as generic terms for the nodes after 3 nm.[29][30] "2-nanometre" (2 nm) and "14 angstrom" (14 Å or 1.4 nm) nodes have also been (in 2017) tentatively identified by An Steegen (of IMEC) as future production nodes after 3 nm, with hypothesized introduction dates of around 2024, and beyond 2025 respectively.[31]

In late 2018, TSMC chairman Mark Liu predicted chip scaling would continue to 3 nm and 2 nm nodes;[32] however, as of 2019, other semiconductor specialists were undecided as to whether nodes beyond 3 nm could become viable.[33] TSMC began research on 2 nm in 2019.[34] It has been reported that TSMC is expected to enter 2 nm risk production around 2023 or 2024.[35]

Helical microtubules of graphitic carbon

Amir Ahdnoparvin, Alexander Alvara, and Charlie Bright

Introduction

On November 1991, Sumio Iijima announced in *Nature* the preparation of **nanometre-size**, **needle-like** tubes of carbon — now familiar as 'nanotubes'.

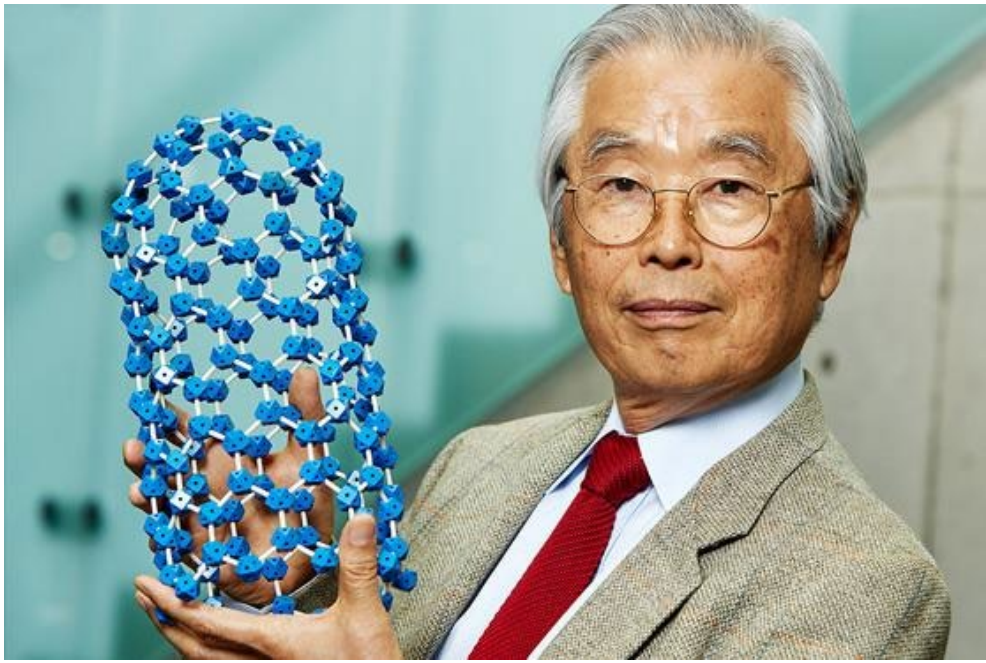

Real Engineering, How Carbon Nanotubes Will change the World

Berkeley
UNIVERSITY OF CALIFORNIA

The Synthesis Process

- Molecular carbon structures **C60**
- graphitic carbon sheets
- Arc-discharge evaporation method

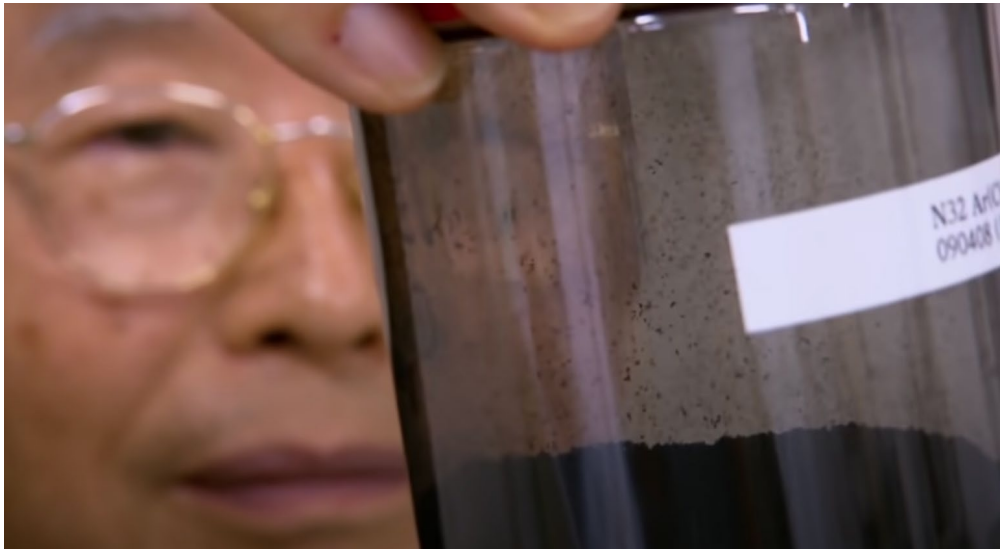

Fullerene

[3]

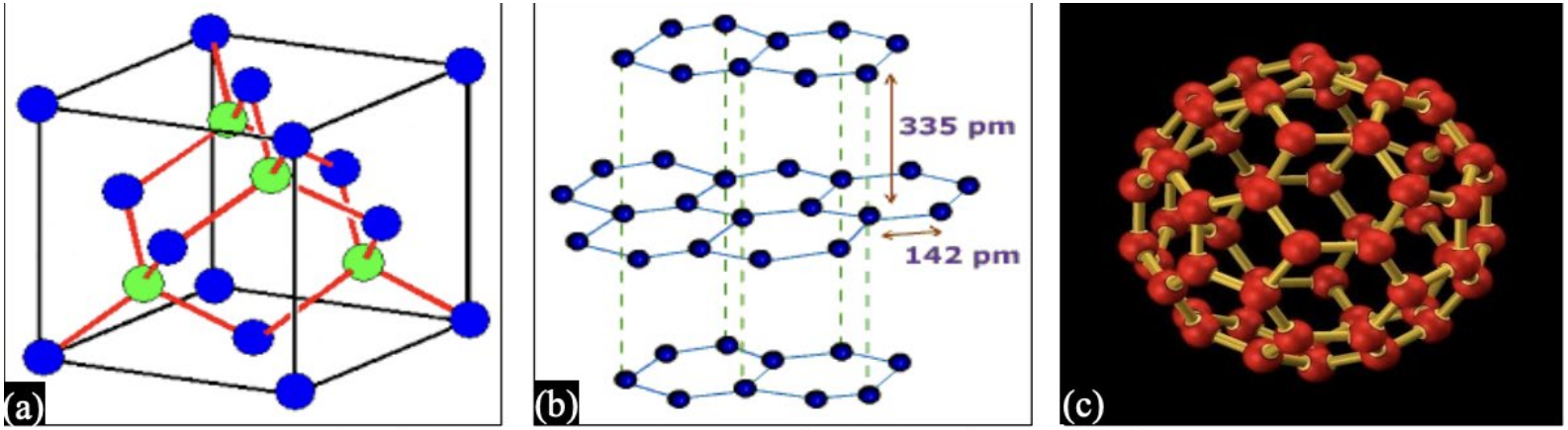

Fig. 1: (a) *Structure of Diamond,* ***(b)*** *Graphite,* ***(c)*** *Fullerene.*

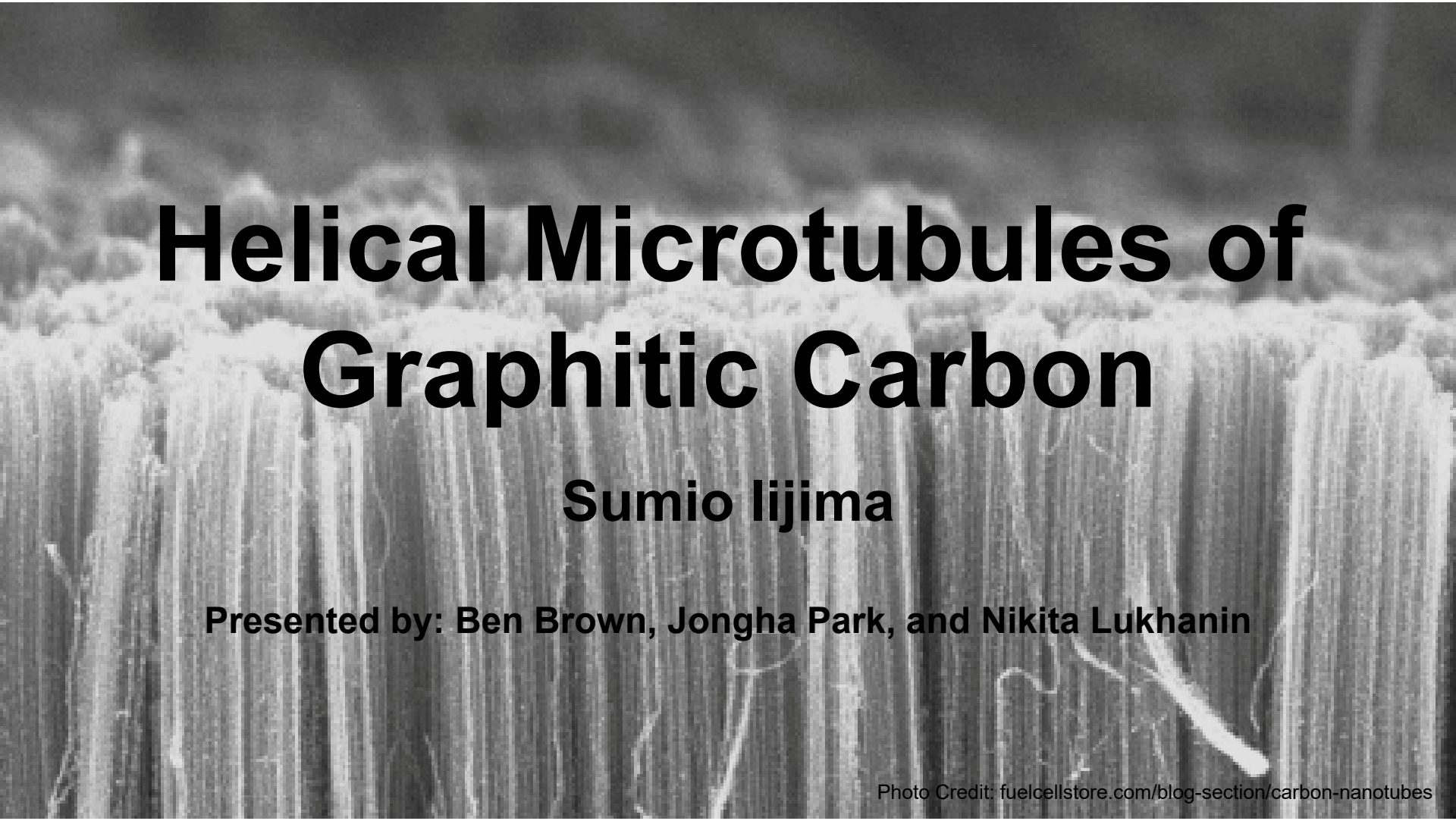

Helical Microtubules of Graphitic Carbon

Sumio Iijima

Presented by: Ben Brown, Jongha Park, and Nikita Lukhanin

Photo Credit: fuelcellstore.com/blog-section/carbon-nanotubes

Introduction

- Inspired off of previous carbon structure work
- Fundamental nanoscience work is presented
- Discusses the invention of carbon nanorods

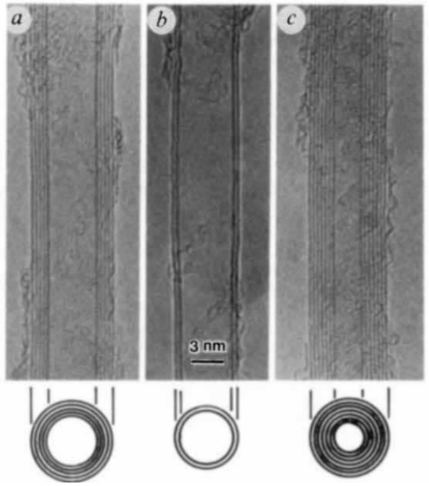

Figure 1. Carbon nanotube electron micrographs

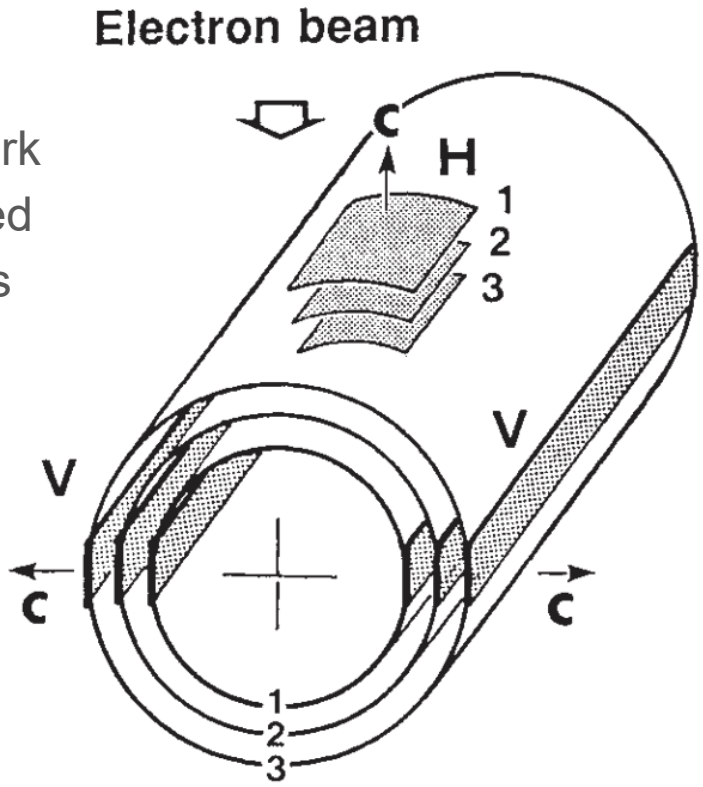

Figure 2. Carbon nanotube diagram

Nikita

Previous Fullerene Work

C60: Buckminsterfullerene

- “Buckyball”
- Won nobel prize in 1996 (Chemistry)
- Not many applications

Figure 3. Buckyball diagram

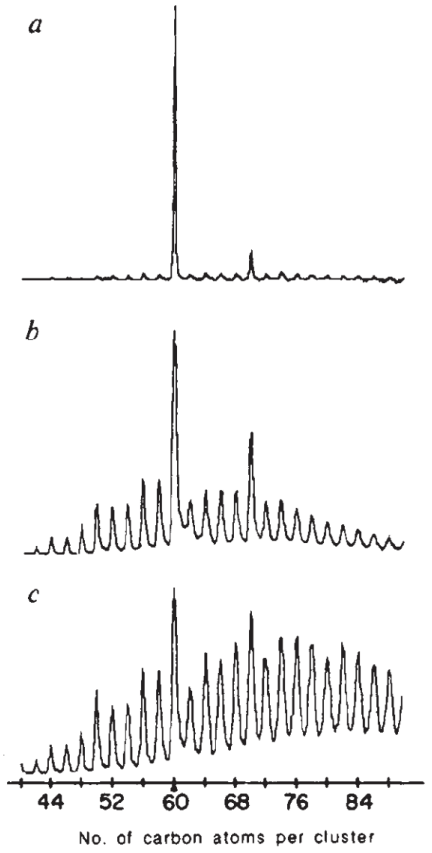

Figure 4. Mass spectrum of vaporised graphene

Nikita

Further Influential Work

- Refined the manufacturing process

- Follow up paper shows the ability to synthesize single wall tubes with 1 nm diam.

- Proposed a method of how nanotubes grow

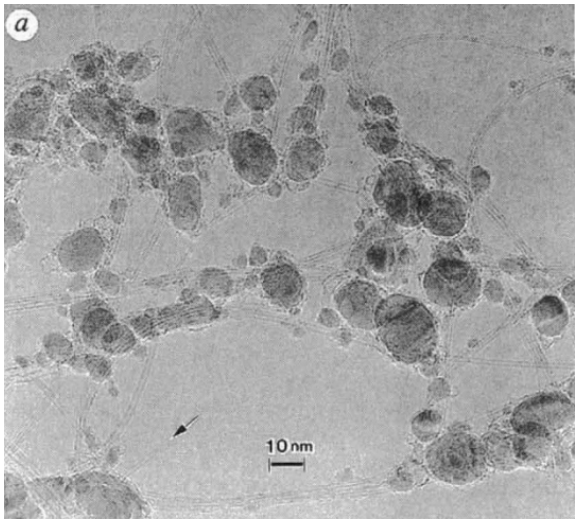

Figure 5. Bundles of carbon nanotubes

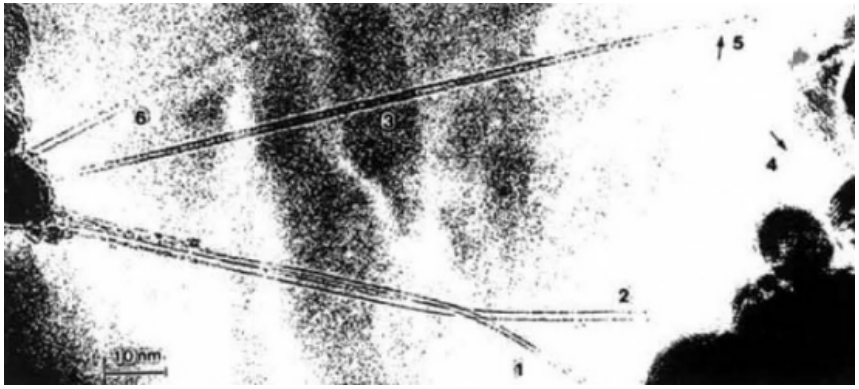

Figure 6. Individual Carbon nanotubes

Nikita

Modern Applications

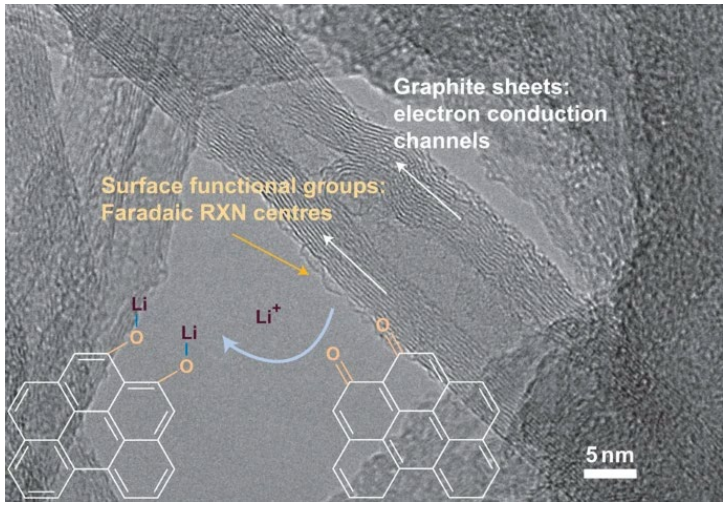

Figure 7. Functionalized nanotubes for batteries

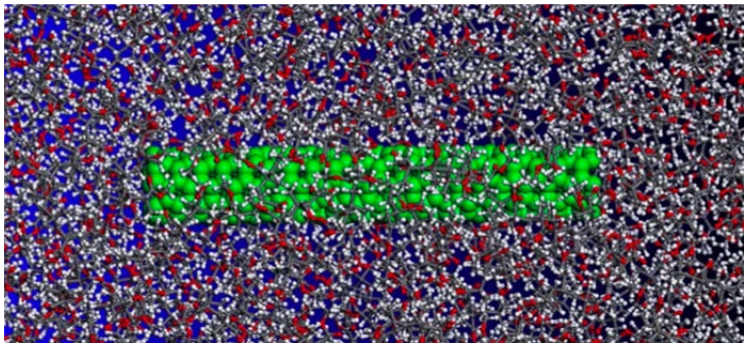

Figure 8. Carbon nanotube within PMMA

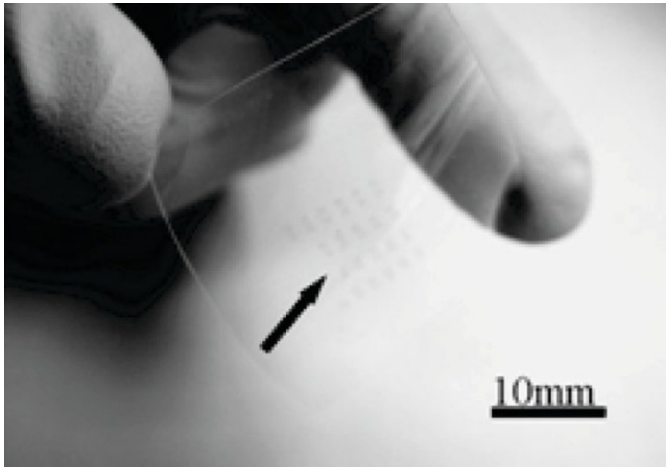

Figure 9. Conductive transparent film composed of nanotubes

Nikita

Fabrication (MWCNT)

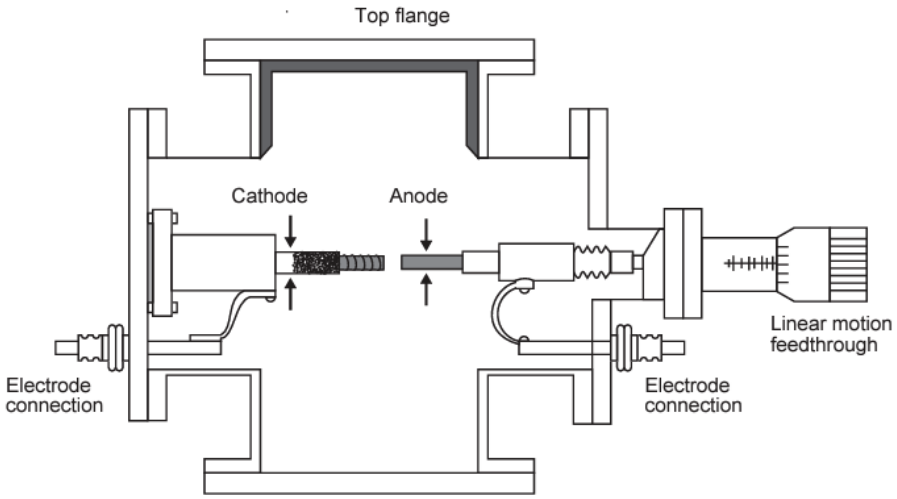

Figure 1. Schematic of Arc Discharge Experimental Setup [1]

- D.C. arc-discharge evaporation of carbon (100 torr Argon)
- Sublimation of carbon by high temperature between electrodes (3000 ~ 4000 ^{o}C)
- Deposited at the negative electrode or the walls of the chamber

Jongha

[1] Carbon Nanotube Reinforced Composites, CNR Polymer Science and Technology (2015)

Fabrication (SWCNT)

Figure 2. Discharge System Used in the Production of SWCNTs [1]

- Single-walled CNT (SWCNT) are doped with catalyst particles
- Ni-Co, Co-Y, or Ni-Y

- Methods of arc discharge generally produce CNTs in grams (expensive)
- CVD produces highest amounts at low prices, but imperfections are common

Jongha

Microscopy

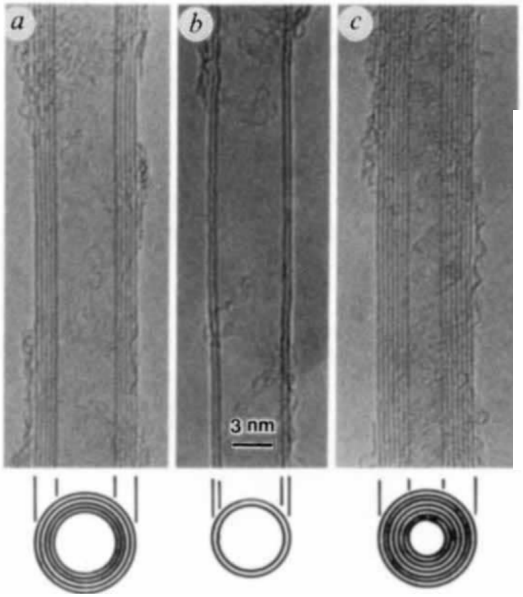

Figure 3. Electron Micrographs of Microtubules of graphitic carbon

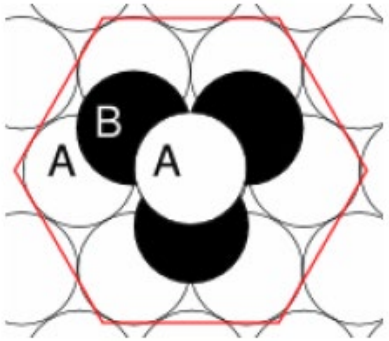

Figure 4. ABAB Hexagonal Stacking Sequence

- TEM (200 keV)
- {002} lattice images along the needle axes
- Fig. 2b: 2 carbon hexagon sheets (0.34 nm)
- Fig. 2c: 2.2 nm in diameter (30 carbon hexagons)
- Imposes strain on the planar bonds of the hexagons (~ 6 ^{o})
- How the ABAB hexagonal stacking sequence found in graphene is relaxed?

Jongha

Electron Diffraction

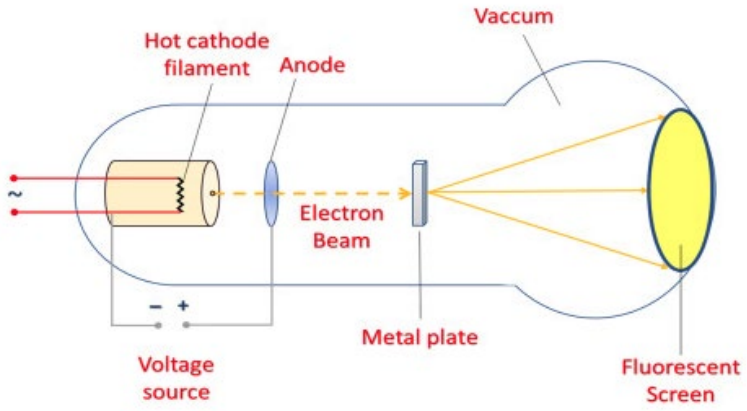

Figure 5. Schematic of Electron Diffraction

- Find crystallographic structural information more precisely
- Fast moving electron beam
- Thin layer of sample
- Observe the diffraction pattern at fluorescent screen

Jongha

Electron Diffraction

- {hk0} patterns show *mm2* mirror symmetry about the needle axis
- (100) and (220) in (a) (three sets of (hk0))
- Two portions of tyc cylinder have same orientation (identical {hk0} pattern

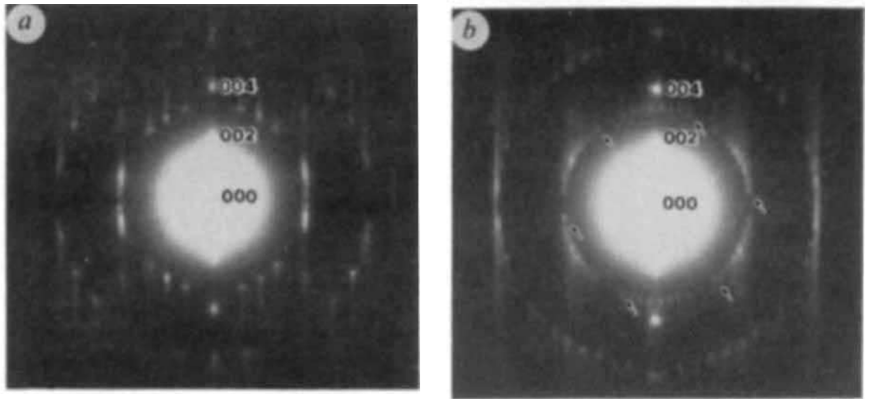

Figure 6. Electron Diffraction Images

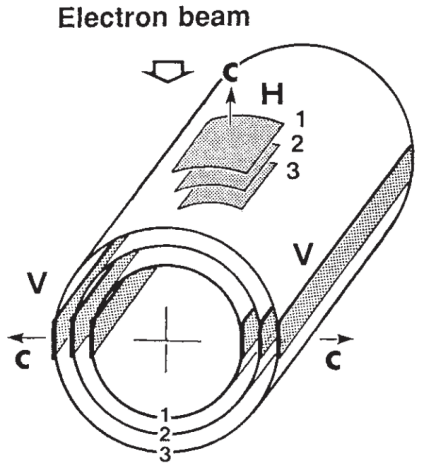

Figure 7. Electron Diffraction Images

Jongha

CNT Structure

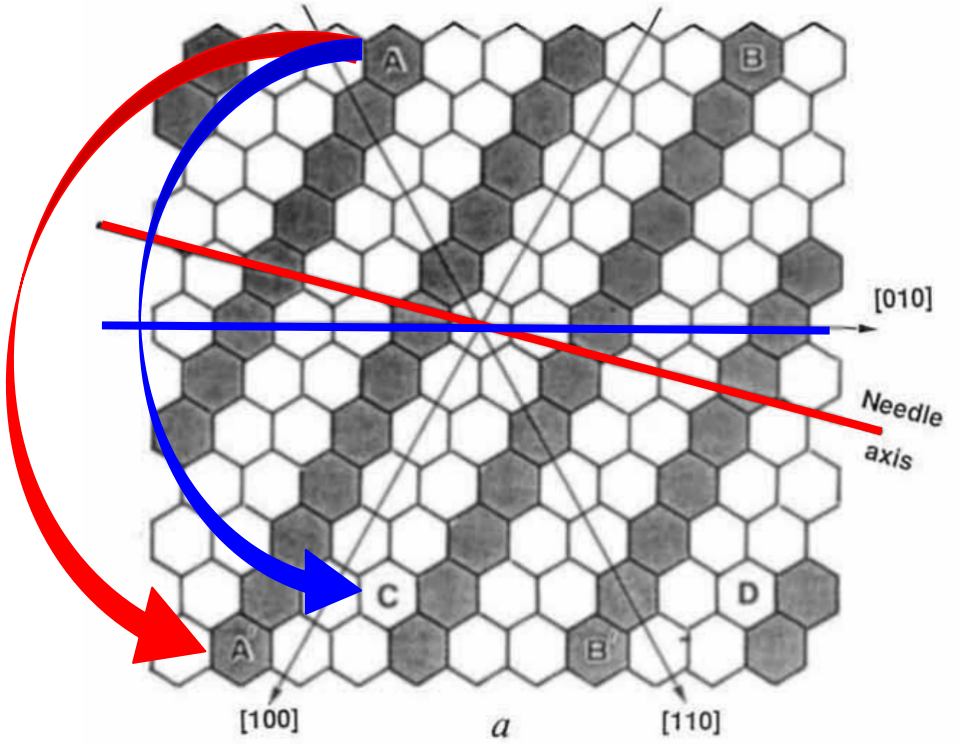

Figure 1. “Unwrapped” structure of helical CNT.

- Structure analyzed through electron diffraction patterns
- sp^2 bonding results in hexagonal structure
- Tubular shape visualized by wrapping graphene sheet around tube axis
- Specific ‘wrapping’ orientation yields different helical structures (chiral angles)

S. Iijima, “Helical microtubules of graphitic carbon,” *Nature*, vol. 354, no. 6348, Art. no. 6348, Nov. 1991, doi: 10.1038/354056a0.

Ben

CNT Ends and Growth

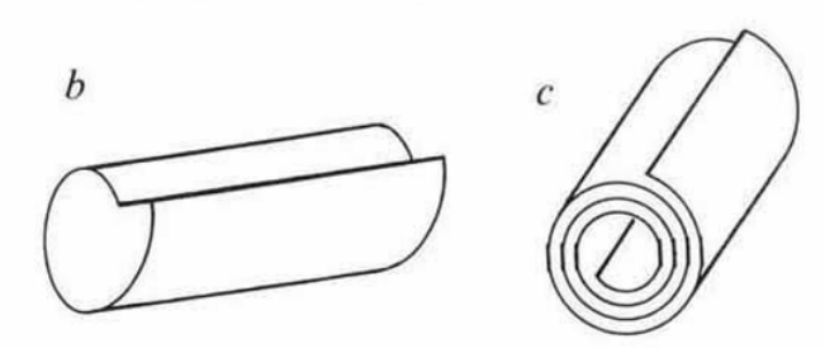

Figure 2. Two proposed CNT growth mechanisms.

Open end model

- Helical configuration
- Spiral growth step
- Observed

Scroll model

- Overlapping edges
- Not observed, concentric cylinders instead

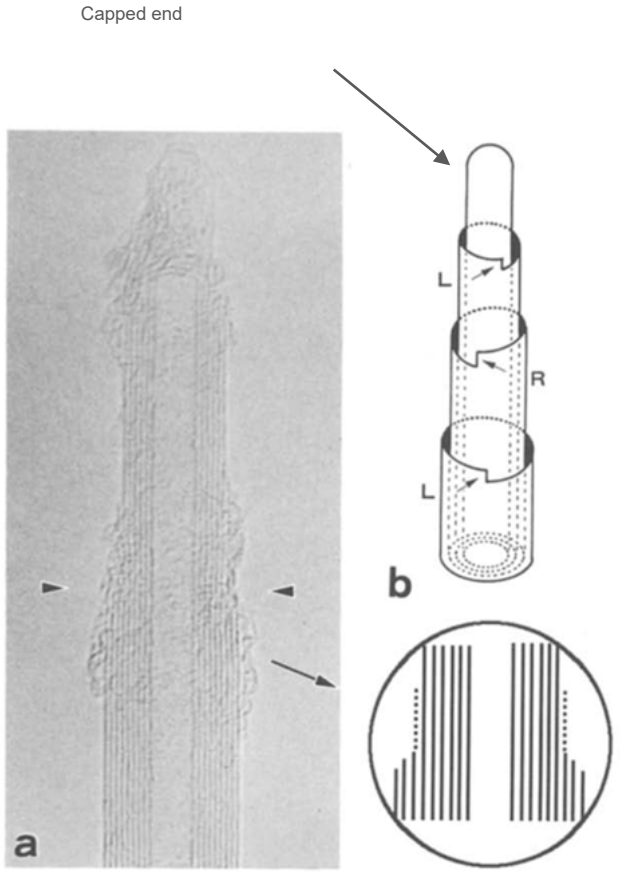

Figure 3. End structure of a CNT.
S. Iijima, “Growth of carbon nanotubes,” *Materials Science and Engineering: B*, vol. 19, no. 1, pp. 172–180, Apr. 1993, doi: 10.1016/0921-5107(93)90184-O.

Ben

CNT Chiral Structures

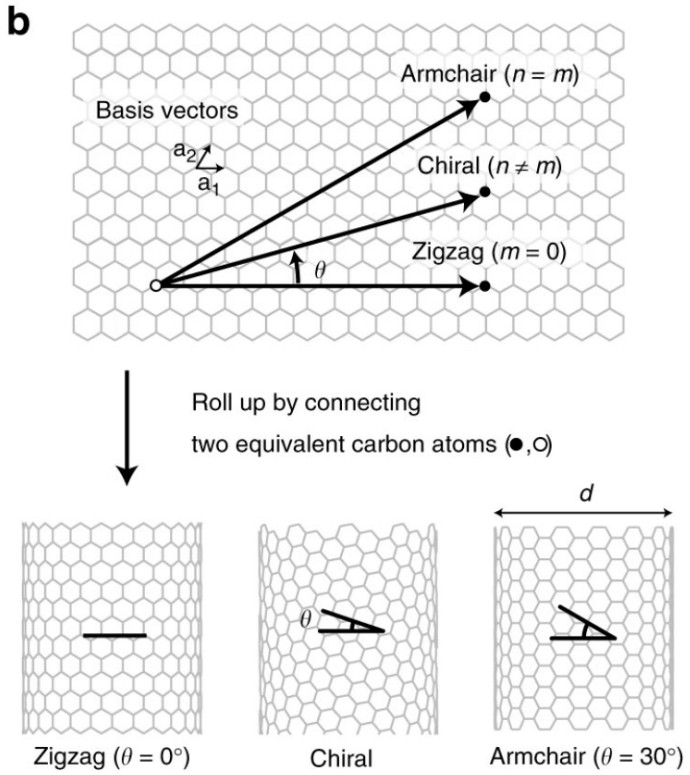

Figure 4. Chiral structure definitions.

- CNT structure defined by diameter and chiral angle
- Chiral angle: angle between hexagon ‘zig-zag’ edge and tube circumference
- Varies from “zigzag” to “armchair”

Ben

A. Takakura *et al.*, “Strength of carbon nanotubes depends on their chemical structures,” *Nat Commun*, vol. 10, no. 1, Art. no. 1, Jul. 2019, doi: 10.1038/s41467-019-10959-7.

Chiral Dependance of CNT Tensile Strength

A. Takakura *et al.*, “Strength of carbon nanotubes depends on their chemical structures,” *Nat Commun*, vol. 10, no. 1, Art. no. 1, Jul. 2019, doi: 10.1038/s41467-019-10959-7.

- There is an effective C-C bond stress than depends on chiral angle and net axial stress
- Failure also depends on stress concentration at defects, which increase in size with diameter

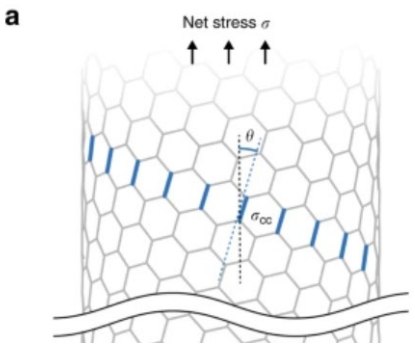

Figure 5. C-C bond stress.

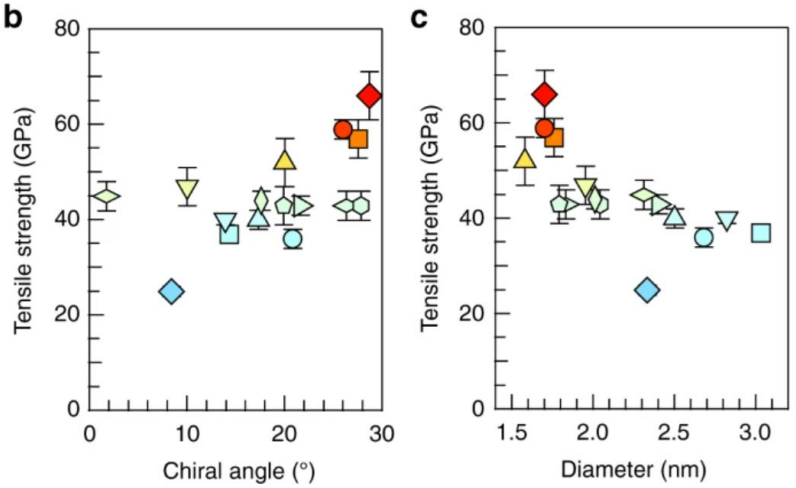

$$\sigma_f = C f(\theta)^{-1} d^{-\alpha}$$

$$\alpha = 0.5 \pm 0.2$$

Figure 6. CNT tensile strength dependence on chiral structure.

Ben

Chiral Structure Control

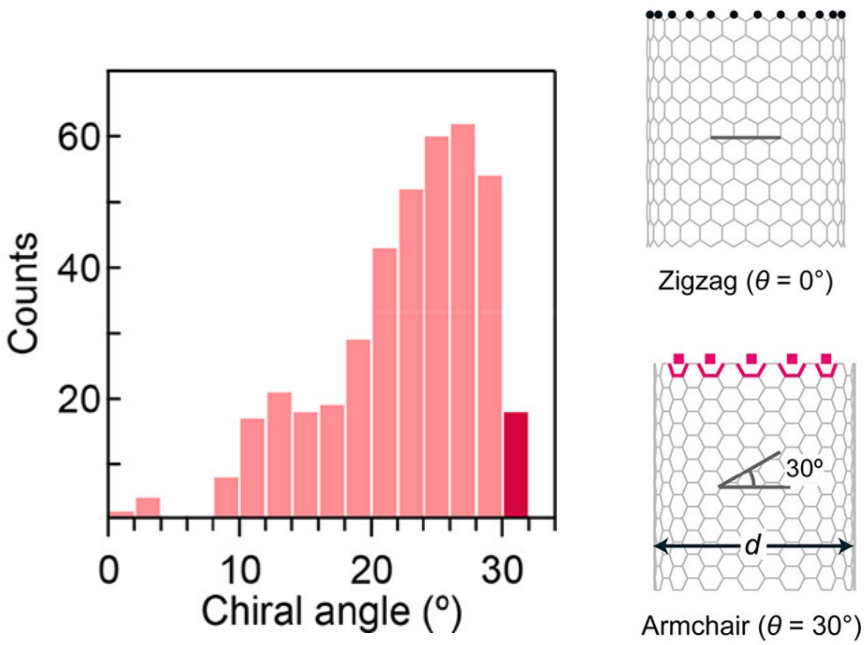

Figure 6. Chiral angle distribution [left] and carbon adhesion site types [right].

- Desire to control CNT properties through chiral structure control
- Extremely small quantities of highly controlled structures achieved
- Goal is to narrow distribution of bulk quantities
- Preferential structures observed
- Due to larger adhesion energy barrier at ‘zigzag sites’ than ‘armchair sites’

T. Nishihara, A. Takakura, K. Matsui, K. Itami, and Y. Miyauchi, “Statistical Verification of Anomaly in Chiral Angle Distribution of Air-Suspended Carbon Nanotubes,” *Nano Lett.*, vol. 22, no. 14, pp. 5818–5824, Jul. 2022, doi: 10.1021/acs.nanolett.2c01473.

Ben

Thank you

Single-shell Carbon Nanotubes of 1-nm Diameter

Sumio Iijima & Toshinari Ichihashi

ME 118/218 Paper 1+: Andrew Cheng, Michael Celebrado, Navin Jeyaselvan

Overview

- Two years since Iijima first published discovery of carbon nanotubes (CNTs)
- Property calculations use single-shell CNTs but carbon-arc synthesis makes multi-shell CNTs
- Knowing the dimension and helical arrangement are important in proving and quantifying properties
- Key takeaways:
  - 1nm single-shell tubes form in the gas phase of a modified carbon-arc setup
  - the helical arrangement can be found with electron diffraction

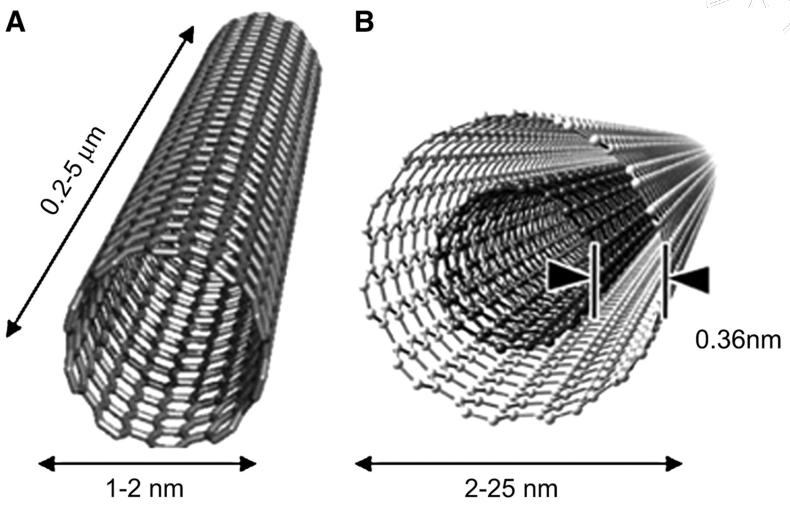

Capillarity

- Proven with liquid lead[1]
- Nanocomposite fibers
- Heating in CO_2 can partially or completely destroy the tube caps and strip outer layers[2]
- Characterized as highly polarizable molecular straws capable of ingesting dipolar molecules[3]

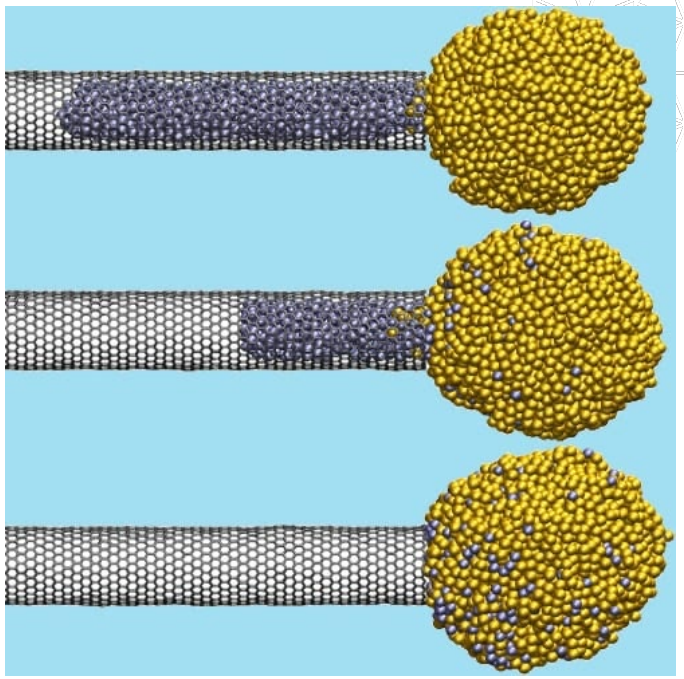

Nanotube Being Used as a Pipette[4]

Electronic Properties

- All predictions and calculations
- Band Structure: Band gaps are metallic to semiconducting depending on diameter and helical arrangement[5]
- Carrier density similar to metal and zero band gap at room temperature
- ⅓ are 1-D metals, ⅔ are 1-D semiconductors[6]

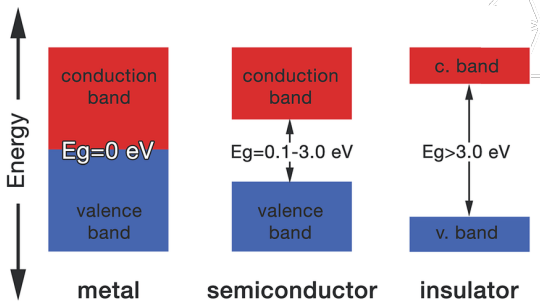

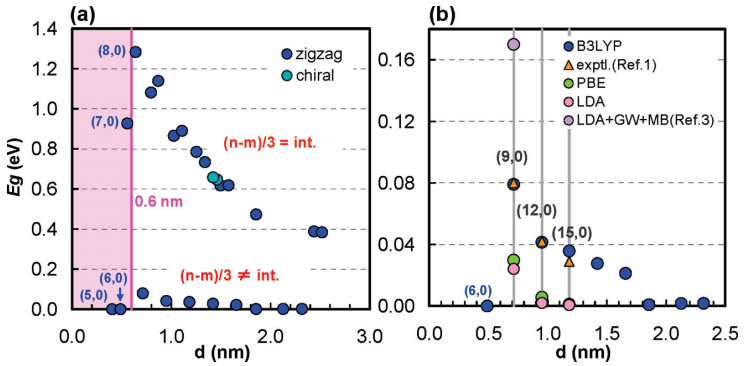

Actual SW-CNT Bandgaps[7]

Berkeley
UNIVERSITY OF CALIFORNIA

Mechanical Properties

- All predictions and calculations[8]
- Strain energy / Carbon atom
  - Varies with $1/R^2$
  - Smaller in symmetric fullerene clusters with similar radii
- Continuum elastic theory relationships can apply here
- Elastic constants dependent on
  - Radius
  - Helical conformation

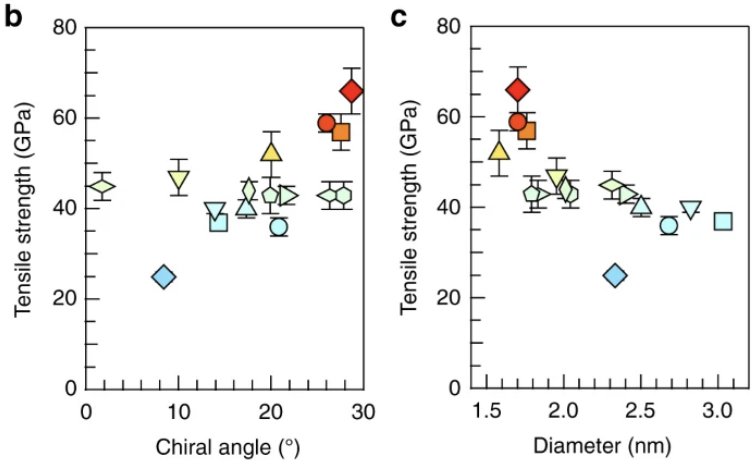

Tensile strength findings of CNTs[9]

Discussion

- Important step in:
  - Deliberate synthesis of single-walled CNTs
  - Further research for empirical evidence of properties
- Limitations
  - Difficult to control the diameter, length, and helical conformation

Nanotube Fabrication

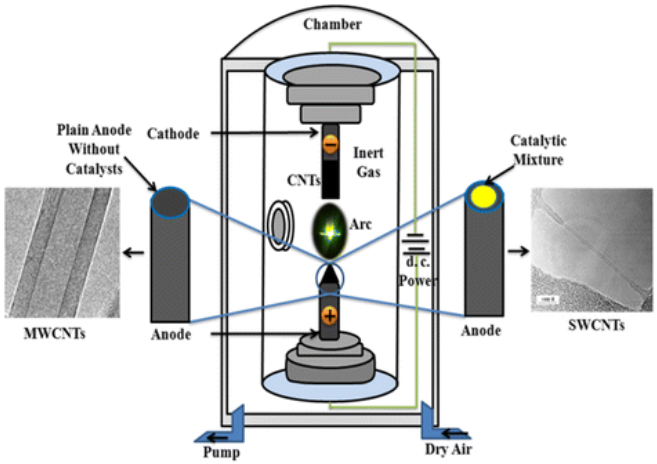

- Carbon-arc chamber
  - Two vertical electrodes
    - Anode (Upper):10 mm graphitic carbon rod
    - Cathode (Lower): 20 mm carbon rod
  - 10 torr methane, 40 torr argon
  - DC current of 200A at 20V
- Iron fillings vaporized
  - Droplet -> Vapor -> Condensation
  - Iron carbide above cathode

Nanotube Fabrication

- Iron has a catalytic role
  - Iron acts as heterogeneous deposition centers in vapor phase
    - Particles found on fiber tips
  - Atomic iron particles as homogeneous catalyst
    - Assists in formation of single-shell tubules
- No tubules in absence of argon, iron or methane

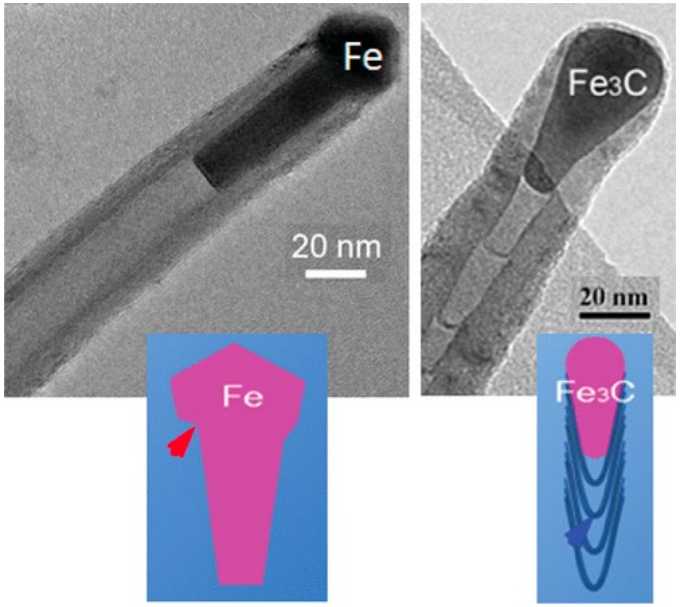

Electron Microscopy

- Transmission Electron Microscope (Topcon 002B)
  - 120 kV/200 kV accelerating voltage
- Performed in ultra-high-vacuum (JEM 200FXV)

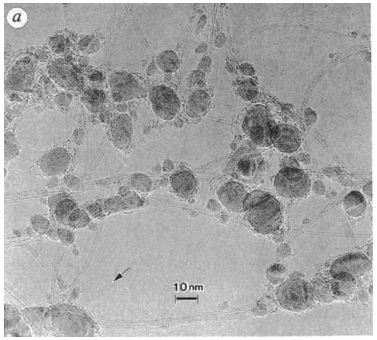

Figure 1a.
Bundles of single-shell carbon nanotubes with cementite particles

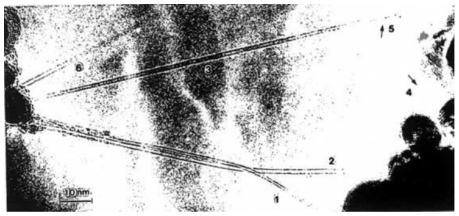

Figure 1b.
Individual single-shell nanotubes

Nanotube Diameters

- Figure 1b shows tubules bridging two cementite particle aggregates
- Micrographs recorded at optimum forces
  - Two dark lines of tubules corresponds to side portion of cylinders

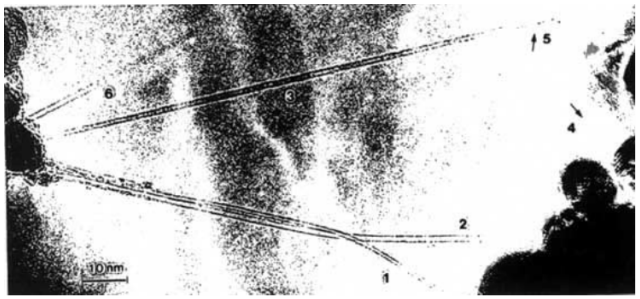

Figure 1b.
Individual single-shell nanotubes

- Thinnest tube (1) with diameter of 0.75nm
  - Attached to thicker, 13nm tube (2)
- Tubules 1,2 curved, tubule 3 (0.92nm) straight across 140 nm opening
- Longest tubule- 700nm long, 0.9nm diameter
- Short, terminated tubules (4, 5)
  - Entangled with cementite particles
- Figure 2- Histogram of diameters of 60 tubules from 0.7nm to 1.6nm
  - Two peaks at 0.8nm and 1.05nm

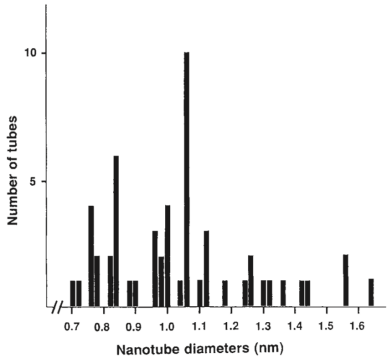

Figure 2
Frequency of single-shell carbon nanotube diameters

Berkeley
UNIVERSITY OF CALIFORNIA

References

1. Ajayan, P. M. & Iijima, S. *Nature* 361, 333–334 (1993).
2. Tsang, S.C., Harris, P.J. F. & Green, M. L. *Nature* 362, 520–522 (1993).
3. Pederson, M. R. & Broughton, J. O. *Phys. Rev. Lett.*, 69, 2687–2692 (1992).
4. Edgar, Kirsten, et al. "Reverse Capillary Action in Carbon Nanotubes: Sucking Metal Nanoparticles out of Nanotubes." *Small* (2011),737–740
5. Hamada, N., Sawada, S. & Oshiyama, S. *Phys. Rev. Lett.* 68, 1579–1581 (1992).
6. Saito, R., Fujita, F., Dresselhaus, G. & Dresselhaus, M. S. *Phys. Rev.* B46, 1804–1811 (1992).
7. Matsuda, Tahir-Kheli, Goddard, The Journal of Physical Chemistry Letters 2010 *1* (19), 2946-2950
8. Robertson, D. H., Brenner, D. W. & Mintmire, J. W. *Phys. Rev.* B45, 12592–12595 (1992).
9. Takakura, A., Beppu, K., Nishihara, T. *et al.* Strength of carbon nanotubes depends on their chemical structures. *Nat Commun* 10, 3040 (2019).
10. Das, R., Shahnavaz, Z., Ali, M.E. *et al.* Can We Optimize Arc Discharge and Laser Ablation for Well-Controlled Carbon Nanotube Synthesis?. *Nanoscale Res Lett* **11**, 510 (2016). https://doi.org/10.1186/s11671-016-1730-0